AN ABSTRACT OF THE THESIS OF

Youran Wei for the degree of Master of Science in Materials Science presented on December 7, 2015.

Title: Characterization of Oxide Growth of Aluminum Alloy 6061 for Nuclear Research and Test Reactors

Abstract approved:_____

Julie D. Tucker   Wade R. Marcum

Oxide growth is a common phenomenon on aluminum alloy cladding surfaces in nuclear research and test reactors. Without better understanding of oxide growth, excessive oxide build up on the cladding surface reduces heat transfer capability from fuel to coolant and causes safety concerns due to the potential cladding rupture or fuel melt. The purpose of this research is to further the understanding of the oxide growth under the operational conditions in nuclear research and test reactors. The four main objectives of this project are to:

1. Extend the existing database for corrosion of aluminum alloy 6061
2. Evaluate the existing correlations for aluminum alloy corrosion under new experimental conditions
3. Help increase the research reactors' operation safety confidence
4. Evaluate the necessity of the pre-filmed boehmite ($AlO(OH)$) layer.

The objectives were accomplished by exposing aluminum alloy 6061 coupons in a test loop operating at low pressure and low temperature. Data from the test loop such as temperature, pressure, pH and exposure time were recorded. SEM (Scanning electron microscope) and ImageJ analysis were used for post experiment examinations to obtain oxide thickness measurement data. Matlab was used to conduct oxide thickness prediction by using existing correlations. Oxide thickness predictions and measurements were compared. EDS (Energy Dispersive Spectroscopy) and XRD (X-Ray Diffraction) analysis were used to identify the oxide chemistry and stoichiometry.

Characterization of Oxide Growth of Aluminum Alloy 6061 for Nuclear Research and
Test Reactors

by
Youran Wei

A THESIS

Submitted to

Oregon State University

in partial fulfillment of
the requirements for the
degree of

Master of Science

Presented December 7, 2015
Commencement June 2016

Master of Science thesis of Youran Wei presented on December 7, 2015.

APPROVED:

_____

Co-Major Professor, representing Materials Science

_____

Co-Major Professor, representing Materials Science

_____

Director of the Materials Science Program

_____

Dean of the Graduate School

I understand that my thesis will become part of the permanent collection of Oregon State University libraries. My signature below authorizes release of my thesis to any reader upon request.

_____

Youran Wei, Author

TABLE OF CONTENTS

TABLE OF CONTENTS (Continued)

LIST OF FIGURES

LIST OF FIGURES (Continued)

LIST OF TABLES

Characterization of Oxide Growth of Aluminum Alloy 6061 for Nuclear Research and Test Reactors

1   INTRODUCTION

1.1   Motivation

In Nuclear Research and Test Reactors (NRTR), aluminum alloys are often used as cladding material for fuel. Subcooled light water is used to remove heat from the fuel during reactor operation. Over time, the aluminum cladding exposed to coolant corrodes and forms an oxide layer. Under operating conditions where the coolant passes next to the cladding at low flow rates the oxide continues to build-up, reducing the heat transfer capability from fuel to the coolant, which acts as a form of thermal insulation. The growing thermal insulation results in an increase in the fuel temperature and cause for attention due to safety concerns resulting from potential cladding rupture or fuel melt. Under high flow rates the coolant may strip this corrosion layer as it grows, thinning the cladding and potentially exposing the fuel material. This too is a matter for attention due to safety concerns centered on fuel release within the reactor. Regardless of the outcome, it is clear that the understanding of oxide growth on aluminum cladding in applicable NRTR is a highly relevant topic for operational safety.

Some NRTR, which utilize light water and aluminum cladding, run with a much higher heat flux than that of operating commercial nuclear reactors in order to perform accelerated experiments. Accelerated testing may enhance the corrosion and increase the fuel temperature. The corrosion rate of aluminum alloys has been studied under high heat flux, high temperature, and high pressure conditions in some reactors such as the High-Flux Isotope Reactor and the Advanced Test Reactor [1-4]. However, the corrosion rate of aluminum alloys has not been studied under low temperature and pressure conditions, which are also important conditions for some NRTR. To predict the rate of corrosion at low temperature and pressure relevant for some NRTR, a new study is required.

1.2 Purpose

Although many studies have been performed to understand the corrosion of aluminum alloys in water under high heat fluxes, low coolant pH values, and high temperature and high pressure [5, 6], there is limited data on the oxidation of aluminum alloys in water with high pH, low temperature and low pressure. Therefore, the purpose of this project is to identify the oxidation rate of an aluminum alloy (6061) under lower temperature and lower pressure conditions, similar to that found in NRTR. Furthermore, the oxidation rate differences due to a pre-filmed boehmite ($AlO(OH)$) layer, which is a particular oxide phase grown on aluminum alloy 6061, on the samples will also be studied. The data obtained during and after the testing campaign includes:

- Water temperature
- Water pH
- Water conductivity
- Pressure
- Experiment time
- Weight changes of samples
- Oxide
  - Thickness
  - Chemical composition
  - Phase identification

Also, metallographic analysis will provide information on the samples' surfaces such as cracks, uniform oxidation layer or pitting. The data will be compared to select previously developed aluminum alloy corrosion correlations to assess their predictive capabilities under experimental conditions considered herein.

An additional goal of this project is to evaluate the necessity of the pre-filmed boehmite layer. The pre-filming process is expensive, and if the results of this project show that it is unnecessary, this could provide substantial cost savings. By having two

types of samples, one with a boehmite layer on the surface and one without, the experiment is testing if the degree of corrosion is similar on these two types of samples. If the amount of corrosion is similar, then the boehmite pre-filmed aluminum alloy will be replaced with non-pre-filmed aluminum alloy, which has a lower fabrication cost.

1.3 Objectives

The objectives of this thesis are to fourfold:

1. Extend existing database for the corrosion of aluminum alloys
2. Evaluate the existing correlations for the new experimental conditions [7]
3. Help increase the research reactors' operation safety confidence
4. Evaluate the necessity of the pre-filmed boehmite layer

The objectives can be achieved by performing the following steps:

- Expose aluminum alloy 6061 coupon samples in a test loop operating at low temperature and low pressure.

- Record experimental data such as temperature, test time, pH and pressure.

- Examine samples after different exposure times in the test loop to measure the oxide thickness and weight change. SEM will be used to measure oxide thickness and for the examination of existence of cracks, pitting and other metallographic features. XRD will be used for phase identification.

- Evaluate the ability of existing correlations, developed for high temperature and pressure, to predict the oxide thickness for the current experimental data conditions.

- Compare corrosion rate of boehmite pre-filmed samples with non-pre-filmed samples.

1.4 Organization of the thesis

This thesis describes the process to accomplish and the results of the stated objectives and is organized as follows: Chapter 2 reviews the existing literature describing reactions of aluminum and aluminum oxide with water, corrosion degree of different

aluminum alloys, effects of different experimental conditions on aluminum alloy corrosion, and correlations of oxide layer thickness prediction. Chapter 3 describes the experimental methods, experimental facilities, sample preparation, data collection and analysis methods used to complete this work. Chapter 4 presents the results and discussion with the comparisons between actual experimental data and the predicted value from correlations. Uncertainty analysis of the measurements is provided for the results. Chapter 5 discusses the conclusions drawn.

2   SURVEY OF LITERATURE

In order to gain a better understanding of the corrosion rate of aluminum alloys and to evaluate the existing corrosion correlations, literature about aluminum alloy corrosion was reviewed. In the literature, reactions of aluminum with water were studied; corrosion correlations used to predict the oxide growth on cladding surface were developed under different experimental conditions, which simulate the operational conditions in reference reactors. A summary of the literature relevant to Al corrosion is presented in this chapter.

2.1   Al corrosion research in non-nuclear industries

Aluminum alloys have unique properties that make them useful to a variety of industries, therefore it is important to have better understanding of aluminum alloy corrosion. Since the main composition of aluminum alloys is aluminum, the study of aluminum is also highly relevant. The key characteristics of aluminum and aluminum alloys are as follows [8]:

- Aluminum is light
- Aluminum alloys have a high strength-to-weight ratio
- Aluminum has good heat and electricity conductivity
- Aluminum has high corrosion resistance under most service conditions

The reason aluminum has a high corrosion resistance is because of the stable oxide layer that forms on its surface once the aluminum is exposed to the atmosphere. The

oxide layer protects the metal from further corrosion unless it's exposed to conditions that disrupt the oxide layer. The high thermal conductivity of aluminum is very important for heating and cooling, it's the reason that aluminum is so commonly used for heat exchanger in many industries [8]. These properties allow aluminum alloys to be used in many applications that require heat exchange, corrosion resistance, and strength.

The three possible reactions of aluminum with water are as follows:

$$Al + 6H_2O = 2Al(OH)_3 + 3H_2 \tag{1}$$

$$2Al + 4H_2O = 2AlO(OH) + 3H_2 \tag{2}$$

$$2Al + 3H_2O = Al_2O_3 + 3H_2 \tag{3}$$

The corrosion product from reaction (1) is aluminum hydroxide bayerite ($Al(OH)_3$). The corrosion product from reaction (2) is aluminum hydroxide boehmite ($AlO(OH)$). The corrosion product from reaction (3) is aluminum oxide (Al_2O_3). All these reactions are thermodynamically possible from room temperature to 660°C. $Al(OH)_3$ is the most stable state from room temperature to 280°C; $\gamma - AlOOH$ is the most stable state between 280-480°C; Al_2O_3 is the most stable state above 480°C [9]. Thermodynamically, aluminum should react with water spontaneously at room temperature. However, the reaction is significantly impeded due to the adhering aluminum oxide layer on the surface, so that aluminum will not react with water at room temperature or even at boiling temperature [9]. The secondary reactions of oxide film on the surface with water are as follows [10]:

$$Al_2O_3 + H_2O \rightarrow 2AlOOH \tag{4}$$

$$Al_2O_3 + 3H_2O \rightarrow 2Al(OH)_3 \tag{5}$$

$$AlOOH + 2H_2O \rightarrow Al(OH)_3 \tag{6}$$

At temperatures below 400°C in air or water, several hydroxides of aluminum will form on the exposed area. When the temperature is below ~77°C, the corrosion

product will be a tri-hydroxide possessing the structure of Gibbsite [$\gamma - Al(OH)_3$], if pH is below ~5.8 or above ~9; Bayerite [$\alpha - Al(OH)_3$] will form, if the pH range ~5.8-~9; or Nordstandite [$Al(OH)_3$] will form, which is often regarded as a mixture of other forms of hydroxides. When the temperature is above ~77°C and below ~102°C, a pseudoboehmite structure is generated, which may aged to other hydroxide forms or remain the same structure. Between ~102°C and ~ 400°C and with pressure below ~2900psi, crystalline boehmite [$\gamma - AlOOH$] will form [10]. Crystalline boehmite has a passivation range from ~pH=4.7 to pH=6.2, where it has good water resistance. Therefore, boehmite treatments are commonly used to increase corrosion resistance of aluminum products. In fact, crystalline boehmite is commonly grown on solid fuel cladding in Advanced Test Reactor (ATR) by treating them with deionized water and high temperature in an autoclave [11].

The corrosion of aluminum, aluminum alloy 6061 and an aluminum-copper alloy was researched in chloride-free and chloride-involving neutral solutions at pH=7 [12]. The principle of aluminum or aluminum alloy corrosion in neutral solutions was based on the dissolution of aluminum atoms provided from the active locations or defected regions on the barrier film naturally formed on them. In oxygen rich aqueous environment, the anodic reactions are [12]:

$$Al_{(s)} + OH^- \rightarrow Al(OH)_{ads} + e^- \tag{7}$$

$$Al(OH)_{ads} + OH^- \rightarrow Al(OH)_{2ads} + e^- \tag{8}$$

$$Al(OH)_{2ads} + OH^- \rightarrow Al(OH)_{3ads} + e^- \tag{9}$$
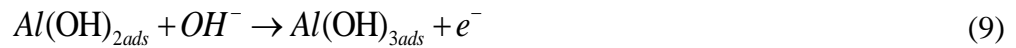
The adsorbed $Al(OH)_3$ would transform into $Al_2O_3 \cdot 3H_2O$ in neutral media, which lead to passivity. The Cl^- ions presented in neutral solutions leaded to the following reactions [12]:

$$Al + Cl^- \rightarrow AlCl_{ads} + e^- \tag{10}$$

$$AlCl_{ads} + Cl^- \rightarrow AlCl_{2ads} + e^- \tag{11}$$

$$AlCl_{2ads} + Cl^- \rightarrow AlCl_{3ads} + e^- \tag{12}$$

$AlCl_3$ hydrolyzed into the solution exposing bare active locations available for corrosion. This explained the increasing corrosion rate when Cl^- ions presented in the solution. For aluminum-copper alloy, the copper presented on the material surface increased the cathodic area and formed a very active galvanic couples, which caused an increase in the corrosion rate. However, it was discovered that the dichromate anion ($Cr_2O_7^{2-}$) effectively inhibited the corrosion process with about 52% inhibition efficiency.

The effect of aging time at low aging temperature on aluminum alloy corrosion was also researched. Localized corrosion of aluminum alloy 6xxx series were affected by the size, type, volume fraction and distribution of the precipitates, which formed under different heat treatment conditions. Precipitates that had significant effect on corrosion were Q-phase ($Al_4Mg_8Si_7Cu_2$) and β'-phase (Mg_2Si). The samples were aged at 225, 185 and 140°C with aging time 42 mins (under-aged), 5h (peak-aged) and 24h (over-aged) [13]. The corrosion current density of samples with different aging time was tested in $NaCl$ solution. The corrosion current density increased with aging time at the beginning and decreased afterwards. Less time was needed to reach maximum corrosion density with lower aging temperature. Corrosion potential shifting was observed for aged conditions. Under-aged samples had susceptibility to intergranular corrosion. For over-aged temper samples, pitting was the primary corrosion type. Coarsening of the precipitates in the grain bodies and grain boundaries was a factor of pitting susceptibility. The complete formation of Q-phase and β'-phase decreased corrosion rate. The peak aged specimens possessed maximum susceptibility to intergranular corrosion [13].

2.2   Al corrosion research in the nuclear industry

Research has been done on the corrosion of aluminum alloys for applications in the nuclear industry. Research was conducted to understand the corrosion behavior of aluminum alloy cladding under different circumstances involving water quality,

temperature, pressure, exposure time, heat flux and different aluminum alloy cladding materials. This research was necessary to study oxide formation on the cladding to ensure safe operation of the reactor.

During reactor operation even in pure water, aluminum alloy claddings can produce relatively thick oxide layers. Water quality is very important for controlling corrosion. If water quality deteriorates for reasons such as poor water source, environmental dirt or corrosion product from material in the reactor system, the aluminum alloy corrosion could be increased. Water quality is characterized by mainly two parameters, pH value of the water and conductivity. At a pH between ~4.5-7, and with conductivity below 1 $\mu S.cm^{-1}$, corrosion of aluminum is minimized [14]. The presence of certain ions will increase corrosion, for instance, chloride ion will strongly motivate corrosion of aluminum alloys.

Four commonly known correlations were used to predict the oxide thickness on aluminum alloys. All of them were developed based on out-of-pile data from loop tests with different tests' conditions. They are known as the Griess, Pawel, Hanson and Kritz correlations.

Griess Correlation

The Griess correlation [1-4] was developed from the data of a series of aluminum alloy corrosion tests in an out-of-pile test loop with the experimental conditions similar to the operational condition in High Flux Isotope Reactor (HFIR) and the Advanced Test Reactor (ATR). The tests were conducted in two groups. The purpose of the first group was to determine the effect of heat flux on aluminum alloy 1100 corrosion. The purpose of the second group was to determine the effect of water pH, temperature and velocity on the corrosion of aluminum alloys (X-8001, 1100, and 6061). The test conditions for these two groups are shown in Table 2.1 and Table 2.2, respectively. Most of the tests were performed at coolant pH 5 and only a few tests were performed at coolant pH 5.7 to 7.0. It was found that coolant pH had a significant influence on the corrosion of aluminum alloys: the higher pH led to a thicker oxide

layer on the cladding surface. Additionally, it was determined that oxide growth was dependent on water temperature and test time. There was no significant difference in the corrosion among aluminum alloys X-8001, 1100, and 6061.

Table 2.1. Griess correlation tests conditions 1 [1]

Characteristic	Location	Value
Flow Rate	Main loop stream [gpm]	80
	Test-specimen cooling channel [gpm]	2.95
	Letdown and feed [gpm]	0.26
	Ion-exchange column [gpm]	0.13
Pressure	Specimen inlet [psia]	370-420
	Pressure drop through specimen [psi]	25
Temperature	Loop [°F]	155
	Specimen inlet cooling water [°F]	155-157
	Specimen outlet cooling water [°F]	191-193
	Average cooling water [°F]	37
Heat Flux	Flow-channel surface under 0.1 inch thick section [Btu-hr^{-1}-ft^{-2}]	1.62×10^6
	Flow-channel surface at edge (0.025 inch thick section) [Btu-hr^{-1}-ft^{-2}]	0.5×10^6

Table 2.2. Griess correlation tests conditions 2 [3]

Test No.	Average Heat Flux (Btu hr-1 ft-2)	Coolant Temperature (°F)		Coolant Flow Rate (fps)	Center Temperature of Specimen(°F)		Pressure (psig)	Alloy	Run Time (hr)	Water Condition (pH)
		Inlet	Outlet		Initial	Final				
A-2	1.7	152	189	41	341	456	300	1100	240	Deionized
A-3	1.63	151	190	37	316	442	900	1100	129	Deionized
A-6	1.7	153	193	38	316	455	900	1100	240	Deionized
A-7	1.58	157	194	38	314	349	900	1100	240	5
A-8	1.58	154	191	37	306	343	900	1100	240	5
A-9	1.57	186	227	35	344	394	900	1100	240	5
A-11	1.57	153	195	33	349	362	900	6061-T6	240	5
A-12	1.51	166	193	51	304	320	900	6061-0	240	5
A-13	1.64	131	173	35	312	320	900	6061-0	240	5
A-14	1.35	190	220	40	337	379	900	6061-0	240	5
A-16	1.55	185	219	41	325	399	60	6061-0	480	5
A-17	2.05	174	218	41	434	440	70	6061-0	240	5
A-18	2.06	174	219	41	391	498	900	6061-0	240	5
A-19	1.93	179	218	41	377	424	80	6061-0	241	5
A-20	2	181	218	42	383	504	920	6061-0	240	5
A-21	2.03	176	220	41	374	578	900	6061-0	240	5
A-22	0.94	198	219	41	316	335	910	6061-0	240	5
A-23	2.05	175	218	41	386	676	900	6061-T6	240	Deionized
A-24	1.65	210	250	37	386	485	950	6061-0	240	5

After analyzing the data, Griess developed the following correlation [4]:

$$x = \varepsilon a \theta^p e^{(\frac{-b}{K})} \tag{13}$$

where

x = oxide thickness, μm,

θ = time, h,

K = surface temperature, K,

a = 443 at pH = 5, constant,

b = 0.778 at pH = 5, constant,

p = 4600 at pH = 5, constant,

ε = 25.4, conversion factor.

Since the oxidation rate was 2.7 times faster when pH of coolant water was 5.7 to 7.0. The constant *a* changes to 1200 from 443 and the other constants remain the same.

Pawel Correlation

The Pawel correlation [5, 6] was developed from the data of aluminum alloy 6061 corrosion tests conducted in an out-of-pile test loop under thermal-hydraulic conditions that were similar to the fuel plate operation conditions in the Advanced Neutron Source (ANS) reactor core. The purpose of these tests was to understand the effect of various experimental conditions on corrosion of aluminum alloy 6061. A subset of data obtained from using conditions similar to those used in ANS was used to develop the preliminary correlation. The test conditions are shown in Table 2.3. From the analysis of the results, Pawel has developed the following correlation [5]:

$$\frac{dx}{d\theta} = \frac{k}{x^n} \tag{14}$$

k can be calculated using equation:

$$k = 6.992 \times 10^5 \cdot e^{[\frac{-7592}{(T_c + 10q)}]} \ \mu m^{1.351}/h \tag{15}$$

where,

$\frac{dx}{dt}$ = rate of layer growth, μm/h;

x = oxide layer thickness, μm;

θ = time, h;

n = constant, 0.351;

T_c = local coolant temperature, K;

q = local heat flux, MW/m².

Assuming the original oxide thickness is x_0, integrating the equation with respect to time θ, with $n = 0.351$, yields the following solution [15]:

$$x_\theta = (x_0^{1.351} + 1.351 \times k \times \theta)^{0.74} \ \mu m \tag{16}$$

where,

x_θ = film thickness at time θ, μm;

x_0 = film thickness at time 0 (θ_0), μm;

k = rate constant, μm$^{1.351}$/h.

The rate constant could be determined using the equation below with a coolant pH of 5 and a range of coolant inlet temperatures between 39 and 52 °C:

$$k = 6.388 \times 10^7 \cdot e^{[\frac{-9154}{(T_c + 1.056q)}]} \text{ μm}^{1.351}/\text{h.} \qquad (17)$$

Plugging k into equation (16) yields the final solution:

$$x_\theta = (x_0^{1.351} + 1.351 \times 6.338 \times 10^7 \cdot e^{[\frac{-9154}{(T_c + 1.056q)}]} \times \theta)^{0.74} \text{ μm} \qquad (18)$$

Table 2.3. Pawel correlation tests condition

Material	Coolant pH	Coolant inlet temperature (°C)	Local coolant temperature (°C)	Local interface temperature (°C)	Local heat flux (MW/m²)	Coolant velocity (m/s)
6061	5	39 to 80	44 to 99	95 to 201	5.2 to 20.2	12.8 to 28

<u>Hanson Correlation</u>

The Hanson correlation [15] was developed from statistical analysis of data obtained by measuring the oxide thickness that formed in an irradiated environment in the ATR and Engineering Test Reactor (ETR). The test conditions are shown in Table 2.4. The statistical analysis used the test results obtained in ATR at 175°F and 250°F to develop the following correlation:

$$x = 2.393 \varepsilon \theta^{0.2578} e^{[\frac{-2412.5}{(K - 273.15) \times 1.8 + 491.67}]} \qquad (19)$$

where,

x = oxide layer thickness, μm,

θ = time, hours,

K = temperature, K,

ε = 25.4, conversion factor.

The standard deviation of the predicting value from this correlation was 31% compared to the measured data.

Table 2.4. Hanson correlation test conditions

Cycle-average oxide surface temperature (°F)		Operation time (h)	Heat flux (Btu /h-ft^2)	Pressure (psig)
ATR	ETR			
250	175	220 to 1150	Up to 2 million	360

Kritz Correlation

The Kritz correlation [16] was developed for the application to Savannah River Production Reactor (SPR). Kritz's correlation has a similar form to the Griess correlation with an additional heat flux term for correction:

$$x = 5208.2 q \theta^{0.778} e^{\left(\frac{-1880}{K}\right)}$$
(20)

where,

x = oxide thickness, μm,

q = heat flux, 10^6 pcu / (hr) (ft^2),

θ = oxide growth time, h,

K = absolute temperature of oxide-water interface, K.

A summary of the test conditions under which the previously discussed correlations were developed are shown in Table 2.5. These correlations were developed under high coolant temperature and pressure with low pH. There were only a few tests that were conducted under pH 5.7 to 7.0. The majority of the tests were performed at pH 5.

Table 2.5. Conditions used to develop correlations

Correlation	pH	Coolant temperature (°C)	Coolant velocity (s/m)	Heat flux (MW/m^2)	Pressure (psig)
Griess correlation	5.0 or 5.7-7.0	121-193	10.67-15.24	4.7-6.3	360 and 900
Pawel correlation	5	T_{local} =44-90	12.8-28	5.2-20.2	NR
Hanson correlation	5	80-121	N/A	6.3	360
Kritz correlation	5	N/A	N/A	5.67-6.5	NR

NR=Not reported

In this project, these existing correlations were used to predict the oxide thickness on the aluminum alloy 6061 coupons in a test loop with experimental conditions such as low temperature and pressure, which were different from the conditions that were used to develop these correlations. By doing this, the veracity of these correlations for new experimental conditions was tested.

2.3 Plot of experimental condition range

Figure 2.1 shows the pressure and temperature ranges used to develop the existing correlations and the temperature and pressure range for this project, data collected from [1, 3-6, 15]. As shown in the figure, the experimental conditions of this project, the purple area, are different from the others. By testing under these conditions, the objectives of extending the existing database of aluminum alloy corrosion and testing existing correlations under new experimental conditions were fulfilled.
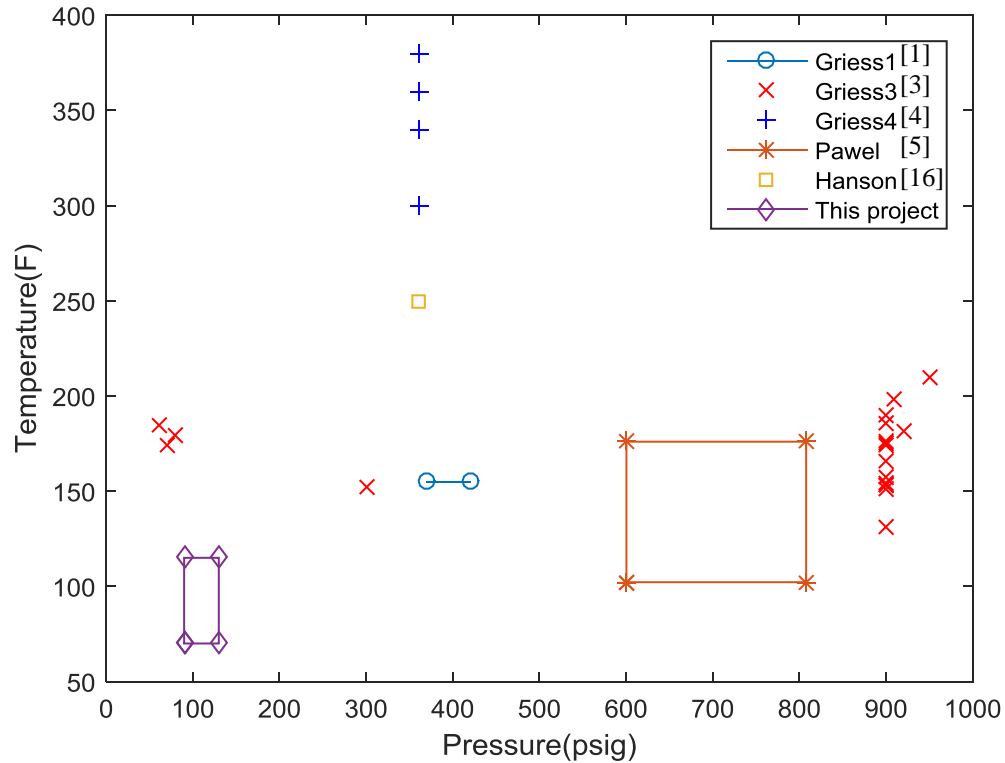
Figure 2.1. Experimental conditions from previous work and this project [1, 3-6, 15]

3 EXPERIMENTAL FACILITIES

3.1 Test loop

The test loop used to expose the 6061 corrosion coupons consists of six systems:

1. Primary coolant system
2. Main feed water system
3. Pressurizing system
4. Water cooling system
5. Coolant recovery system
6. Air system

The facility, located in Radiation Center in Oregon State University, is shown in Figure 3.1. The accumulator tank from the pressurizing system was used as the corrosion coupon test chamber in the project. In the pressurizing system, the installed instruments include: pH and conductivity probes to provide the pH and conductivity values, a level switch to indicate whether there is sufficient water in the accumulator tank, and a thermocouple to provide the fluid temperature in the tank where the

coupons were placed. A compressor was used to maintain the pressure between 90 to 130 psig. The water-cooling system controls the temperature of the coolant. Test conditions used in the test loop are shown in Table 3.1.

Figure 3.1. Test loop facility

Table 3.1. Test conditions for this project

pH	Temperature (°F)	Conductivity (μS/cm)	Pressure (psig)
6.6-8.0	70-115	~124	90-130

3.2   Samples description

The material of the coupons in this project is aluminum alloy 6061. The composition of this alloy is shown in Table 3.2.

Table 3.2. Typical composition of aluminum alloy 6061 composition [17]

Aluminum alloy	Mg	Si	Fe	Cu	Zn	Ti	Mn	Cr	Others	Al
6061	0.8-1.2	0.4-0.8	Max. 0.7	0.15-0.4	Max. 0.25	Max. 0.15	Max. 0.15	0.04-0.35	0.05	Balance

Two types of coupons were prepared. One type was pre-filmed with an oxide layer and the other type received no pre-filming. Coupons were labeled with numbers and letters B or N, which represented boehmite pre-filmed and non-pre-filmed, respectively. A representative picture of coupons is shown in Figure 3.2. The average surface roughness for pre-filmed coupon was 0.17 μm with a 0.02 μm standard deviation. The average surface roughness for non-pre-filmed coupon was 0.27 μm with a 0.04 μm standard deviation. Round coupons were punched from aluminum alloy 6061-T0 plates of both types of samples. The pre-filmed plates form a boehmite layer in the autoclave, so that the surface of the pre-filmed coupon had a uniform boehmite layer on both sides, however, the rim of the coupon did not have an oxide layer. Both types of coupons had the same diameter of 1.25 inches. The pre-filmed coupon was 0.102 inch thick. The non-pre-filmed coupon was 0.051 inch thick. Each coupon had a 0.25-inch diameter hole close to the edge in order to hang them on a rod.

Figure 3.2. Boehmite pre-filmed coupon (left) and non-pre-filmed coupon (right)

The coupon-labeling scheme is shown in Appendix A. The 24 pre-filmed coupons and 21 non-pre-filmed coupons were hung on two separate ceramic rods, which were fixed on two test trains. Each coupon on the rod was separated with a ceramic nut. At least one of each type of coupons was extracted from the trains per month for analysis. Extra coupon extraction was needed based on the examination requirement. A picture of the trains with coupons mounted is shown in Figure 3.3.

Figure 3.3. Coupon trains with coupons

These coupons needed preparation for Scanning Electron Microscopy (SEM) analysis. After exposure in the test loop, a small piece was cut off from the coupons using a slow speed saw with a diamond blade. Then, the piece was mounted in bakelite with the cross-section facing up on the mount surface. Next, the samples were polished using sandpaper and polishing wheels. Last, the samples were cleaned by water and dried using compressed air. Figure 3.4 shows an example of prepared cross-section sample. The rest of the coupon, as shown in Figure 3.5, was cleaned with soap water and water for surface analysis. The details about sample preparation can be found in Appendix A.

Figure 3.4. Prepared cross-section sample from a pre-filmed coupon

Figure 3.5. A non-pre-filmed coupon after a sectioning

3.3   Data collection and analysis methods

3.3.1   Overview of data collection methods

The data acquired during the tests were bulk coolant temperature, coolant pH, coolant conductivity, system pressure, operation time, and a binary 1-0 value recorded to indicate the water level. All types of data were recorded every 15 minutes from the test loop and input into an Excel file for further analysis.

In the post examination of exposed coupons, many methods were applied to obtain the critical data and identify important information. The coupons' weight changes after tests were examined by microbalance.   SEM analysis was applied to obtain the metallurgy information such as cracks, pitting, internal oxidation, oxide deposits, spallation, and oxide thickness. Energy Dispersive Spectroscopy (EDS) was used to collect chemical composition information of oxide layers and deposits. X-ray Diffraction (XRD) analysis was used to determine the oxide layer crystal structure. The test matrix is shown in Table 3.3, which indicates the arrangement of all the methods mentioned above.

Table 3.3. Test matrix

Month	# of coupons	Analysis conducted	Additional comments	Sample ID
Original coupons	1 for each	Weight measurement(with and without deposit), XRD(surface), SEM(surface, cross-section)		B(boehmite):1 N(Non pre-filmed):1
First month	1 for each	Weight measurement(with and without deposit), SEM(surface and cross-section),EDS on deposit,		B:2 N:2
Second month	1 for each	Weight measurement(without deposit),SEM(surface and cross-section), EDS(oxide layer, and EDS map for the surface),		B:3 N:3
Third month	1 for each	Weight measurement (with and without deposit),SEM(surface and cross-section), EDS(oxide layer, sample body),	Clean the sample with ultrasonic device. Possibly because of using ultrasonic device, some oxide layer were knocked off.	B:4 N:4
Fourth month	1 for each	Weight change(with and without deposit), SEM(surface and cross-section), XRD (surface), EDS(oxide layer and deposit)	Water chemical analysis	B:5 N:5
Fifth month	2 for each	Measurement(with and without deposit), SEM(surface and cross-section), XRD (surface), weight EDS(oxide layer)	Extra coupons are for XRD surface analysis	B:6,7 N:6,7
Sixth month	2 for each	Weight measurement(with and without deposit), SEM(surface and cross-section)	EDS on the oxide layer if the chemical composition is not certain at this time	B:8,9 N:8,9

3.3.2 Weight change analysis

The weight change of coupons was measured using a Sartorius ME36S Microbalance. It is a very sensitive scale that has an accuracy of ± 1µg. Before the coupons were put inside the test loop, the mass of each coupon with corresponding labeled tray was measured three times and the average values were calculated. Therefore, the measuring error was minimized. After exposure, coupons were dried in the corresponding labeled plastic trays for 7 days. By putting the coupons in the tray, weight loss from oxide falling off the surface was avoided. Each coupon with its corresponding tray was measured three times. The coupons' weight gains were obtained by subtracting the weight before exposure from the weight after the exposure.

3.3.3 SEM-EDS analysis

SEM is an important method to obtain sample images, which were used in the following analysis to measure the oxide thickness. SEM-EDS was also a main method to obtain the sample's oxide chemical compositions. To improve the quality of the SEM images, the prepared samples were fixed on a stud with metal adhesive tape to increase the sample's electrical conductivity. For each sample's cross-section, eight images were taken from eight evenly distributed locations on both sides of the sample. To make data consistent and minimize error, all images were taken at 3500X magnification. An image of original pre-filmed sample is shown in Figure 3.6. The oxide layer is clearly shown in the middle of the image. Also any defects presented in the oxide layer could be easily detected. When taking the image, a screen rotation was applied to ensure the oxide layer was always horizontal in the picture to make future analysis easier. Other images of cross-sections were taken to show some defects of the oxide layer to help explain some experimental phenomenon. These figures can be seen in result section and in Appendix B. Images of the coupon surfaces were also taken by SEM to determine the shape and distribution of oxide.
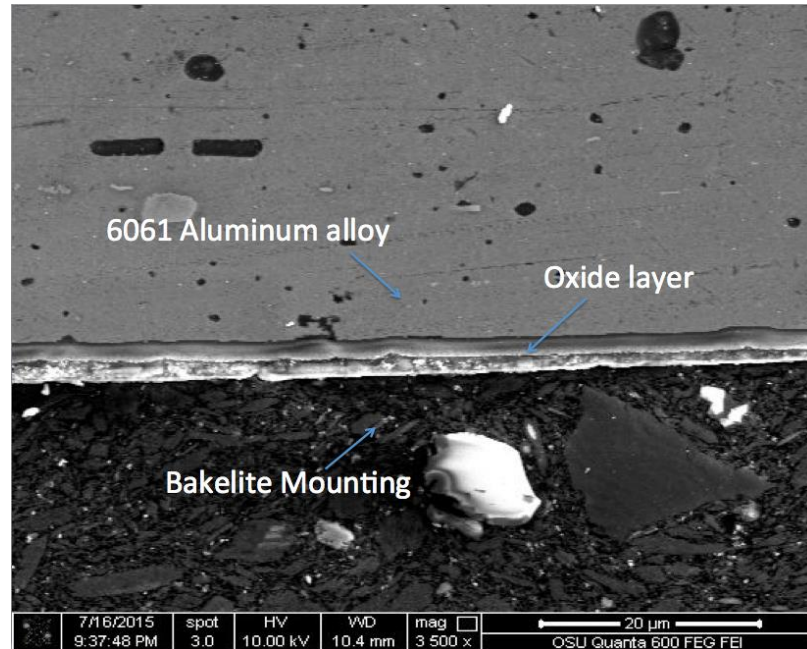
Figure 3.6. Cross-section image of original pre-filmed coupon

The SEM images of oxide thickness were analyzed using the ImageJ software. The measuring process is demonstrated in Figure 3.7. ImageJ can be used to measure the length and area in a picture after setting the scale. To set the scale, a distance of known length in the image must be defined. The scale bar in the SEM image can be used to set the scale in ImageJ. In this project, the 'freehand selection' tool was used to identify the total area of the oxide. Therefore, the average oxide thickness in the image was calculated by dividing the total oxide area by the length of the oxide layer. The image was rotated to horizontal referring to the scale showing on the screen to reach the maximum horizontal degree. The horizontal field width (HFW) value was used as length of oxide layer. This process was repeated for all eight images, then the average oxide thickness of that sample was determined as the average value of oxide layer thickness from eight images.
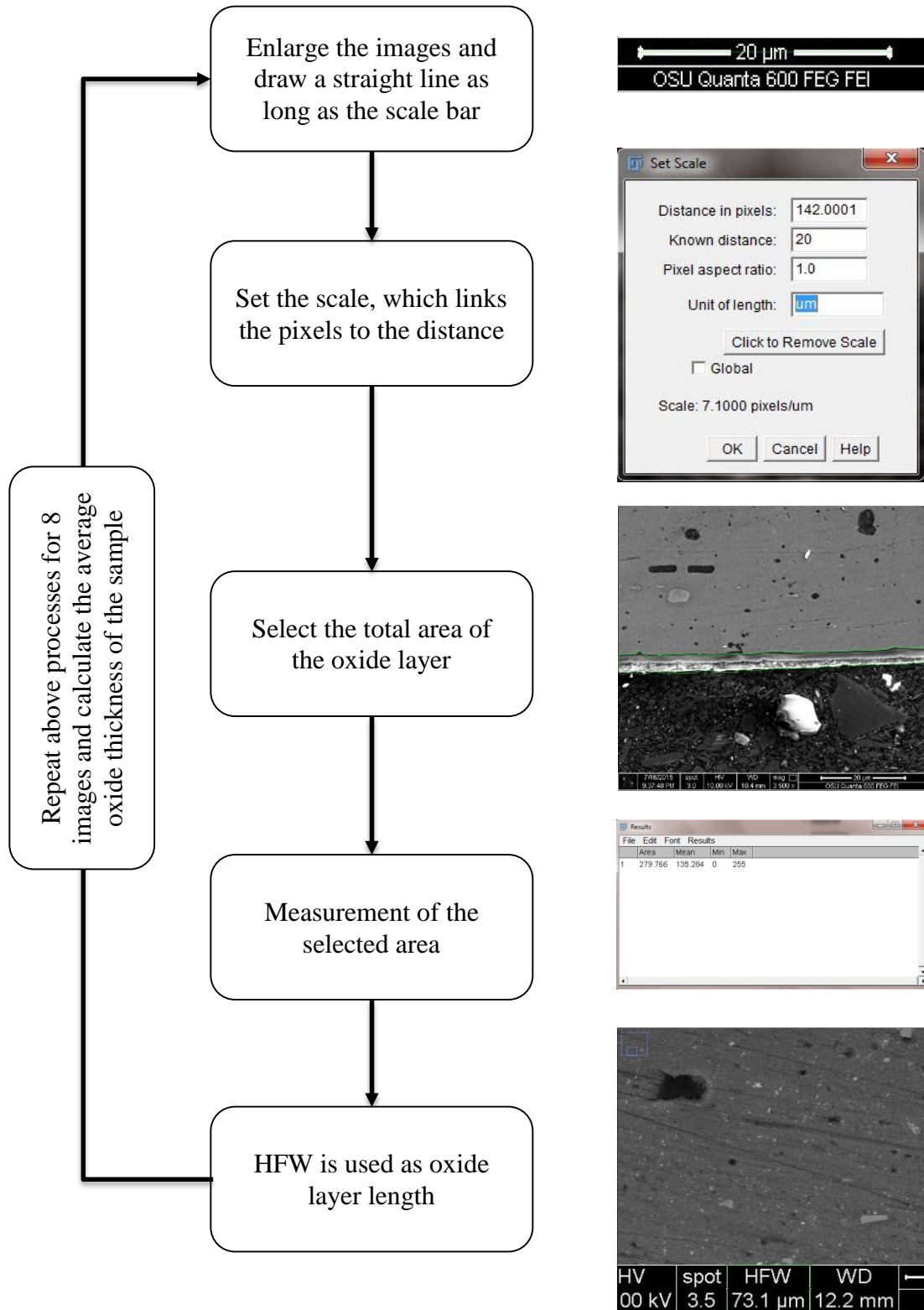
Enlarge the images and draw a straight line as long as the scale bar

Set the scale, which links the pixels to the distance

Select the total area of the oxide layer

Measurement of the selected area

HFW is used as oxide layer length

Repeat above processes for 8 images and calculate the average oxide thickness of the sample

Figure 3.7. Flowchart of ImageJ for measuring oxide thickness

3.3.4   EDS analysis process

Energy Dispersive Spectroscopy (EDS) is a characterization technique of SEM. It provides chemical composition analysis based on X-ray spectra generated from an area scanned by primary electrons. The device can detect the counts (incident X-rays converted to electric signals by semiconducting detector) and the energy level of those counts. EDS software can associate the energy level of the X-rays with the elements that generate them. In this project, EDS analysis was used to determine the chemical composition of the deposits that formed sporadically on the top of the oxide layer and the chemical composition of the oxide layer that formed uniformly on the coupon surface. Since the oxide layer and deposit were both aluminum alloy corrosion products, the main elements of interest were aluminum and oxygen. Therefore, the appropriate voltage for the analysis was determined to be 3kV. Spot electron and amplify time are two adjustable parameters in the software. By adjusting those two parameters, dead time percent (DT) and counts per seconds (CPS) in the EDS software had appropriate value, which was 20-40% for DT and over 1000 for CPS, respectively. A data collection time of 60 seconds was enough to produce a good EDS result. If DT and CPS weren't able to adjust into the ideal range, increasing the data collection time properly was still able to collect adequate intensity in order to provide a good result.

3.3.5   XRD analysis

XRD analysis provides crystal structure information that can be used to determine the type of oxide layers and deposits that were forming on the samples. XRD analysis was conducted using Bruker D8-DISCOVER analytical and cabinet X-ray machine. The samples were placed on the stage horizontally. Since the deposit could not be completely cleaned off from the coupon's surface, a nozzle was installed on the X-ray equipment to reduce the scan area. Therefore, the scan area was limited to only the oxide layer. Since the structure of the objective substance for this project has strong peak at 14° (2θ). And there were some other peaks showed up towards the 80°. Therefore the scanning angle, which was 2θ, was chosen from 10° to 80° Scanning rate was set at 1 degree per second since at this rate it provided the peaks that contain sufficient information to do analysis.   The scan results were analyzed by EVA

software. EVA was used to identify peaks and search for results. In the search results, EVA provided the best possible structures that could contribute to the shape of the peaks in the scan result. Once one structure was selected from the search result, the peaks for that structure was compared with the peaks from scan result. From the comparison, the structures that had the most similar peak trends were inferred as the oxide layer structure.

3.3.6 Method of Using Correlations

In this project, the coolant temperature, pH, conductivity, and system pressure were recorded. No heat flux was generated in the loop, therefore the Kritz correlation couldn't apply to this project. However, the Griess, Pawel and Hanson correlations were appropriate for this project. Since no heat was generated from the coupons, the temperature across the coupons was the same as the coolant temperature.

For the Griess correlation, since the pH of the coolant was around 7.5, the value of constant "a" was 1200. Temperature data recorded by the test loop was converted into Kelvin in order to use in the correlation. The Griess correlation was modified, so that the total oxide thickness at each data point was calculated by the following equation:

$$x_i = \varepsilon\{x_{(i-1)} + 1200[\text{Time}_{(i)}^{0.778} - \text{Time}_{(i-1)}^{0.778}]e^{(\frac{-4600}{K})}\} \qquad (21)$$

where,

x_i = total oxide thickness at $Time_{(i)}$ (µm),

$x_{(i-1)}$ = total oxide thickness at $Time_{(i-1)}$ (µm),

$Time_{(i)}$ = total exposure time at i^{th} data point,

ε = 25.4, convertion factor

K = surface temperature (K).

Normally $Time_{(i)} - Time_{(i-1)}$ = 15 minutes, however, there were situations in which the recording system didn't follow that rule. The actual time difference was calculated between each data point.

For the Pawel correlation, the time parameter and temperature parameter were used the same way as it was used in the Griess correlation. However, a term representing the existing oxide thickness was involved in the Pawel correlation. Therefore, the total oxide thickness was calculated by following equation:

$$x_i = (x_{(i-1)}^{1.351} + 1.351 \times k \times [\text{Time}_{(i)} - \text{Time}_{(i-1)}])^{0.74} \text{ } \mu m \tag{22}$$

where,

$$k = 6.388 \times 10^7 \cdot e^{[\frac{-9154}{(T_c + 1.056q)}]} \mu m^{1.351}/h,$$

$$T_c = \text{local temperature (K)},$$

$$q = \text{heat flux (MW/m}^2).$$

For the Hanson correlation, time data was used in the same way as it was used in the Griess and the Pawel correlations. The total oxide thickness was calculated by following equation:

$$x_i = x_{(i-1)} + 2.393\varepsilon(\text{Time}_{(i)}^{0.2578} - \text{Time}_{(i-1)}^{0.2578})e^{[\frac{-2412.5}{(K-273.15)\times 1.8 + 491.67}]} \tag{23}$$

4   RESULTS AND DISCUSSION

In this section, results of numerous analysis methods are presented. SEM images of samples from each month are presented. Representative oxide layers for both types of samples are shown in the images below. Defects such as pitting, broken oxide layer, and excessive oxidation were detected in the SEM images. Results of average oxide thicknesses were obtained based on SEM images by using ImageJ software. Predicted oxide thicknesses were calculated by Matlab using appropriate correlations. Plots containing predicted thicknesses and measured thicknesses were made by Matlab script for comparison and discussion. Results of EDS and XRD analysis were used to infer the oxide substance.

4.1   SEM results

The oxide thickness for each month of exposure was determined from cross-section sample images taken by SEM. Figure 4.1 and Figure 4.2 show representative images of cross-section samples from each month on pre-filmed coupons and non-pre-filmed coupons, respectively. The full list of images can be found in Appendix B.
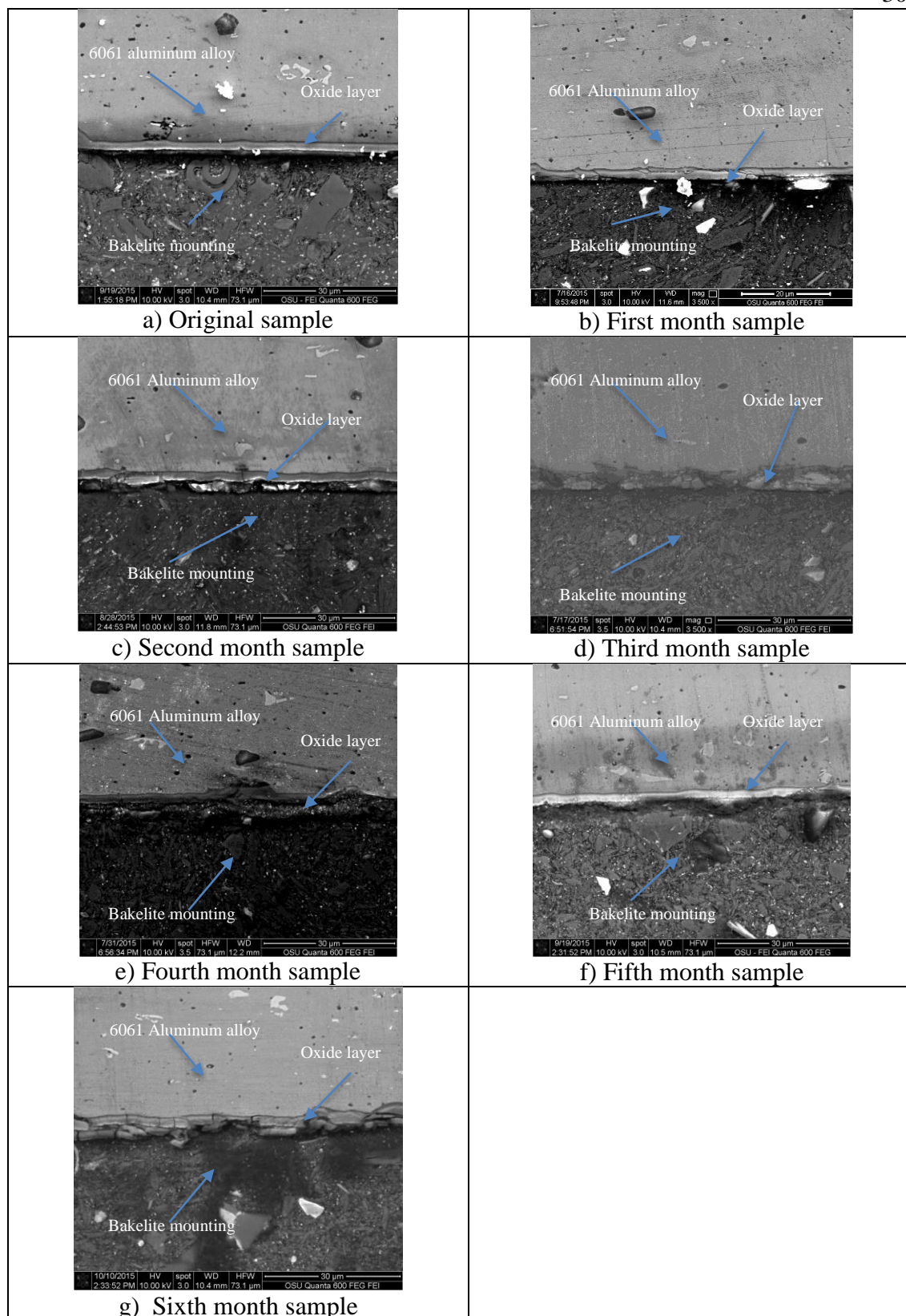
a) Original sample

b) First month sample

c) Second month sample

d) Third month sample

e) Fourth month sample

f) Fifth month sample

g) Sixth month sample

Figure 4.1. SEM cross-section pictures of boehmite pre-filmed samples

a) Original sample

b) First month sample

c) Second month sample

d) Third month sample

e) Fourth month sample

f) Fifth month sample

g) Sixth month sample

Figure 4.2. SEM cross-section pictures of non-pre-filmed samples
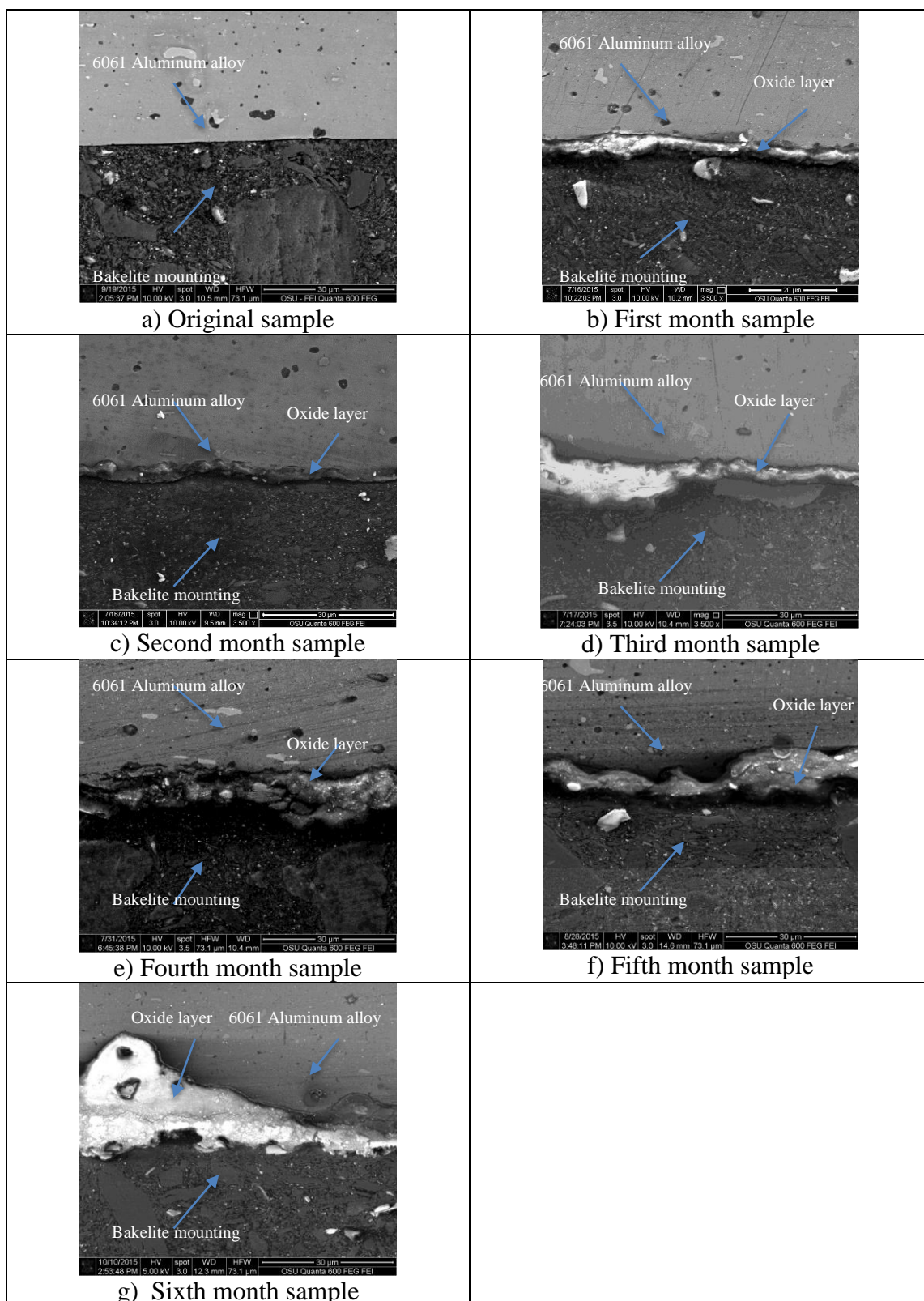
Figure 4.1 and 4.2 show that, in general, the oxide layer on the pre-filmed samples had a more uniform formation than that on the non-pre-filmed samples. The average oxide thickness values obtained by ImageJ, as shown in Table 4.1, proved that the average oxide thicknesses on pre-filmed coupons was thinner than that on the non-pre-filmed coupons after 2 months of exposure. Therefore, it's reasonable to infer that non-pre-filmed coupons have a greater corrosion rate in the test loop than the pre-filmed coupons. The only difference between these two types of coupons is the pre-filmed boehmite oxide layer. The conclusion drawn from this is that the pre-filmed oxide layer helps reduce the oxide growth in the test loop. It is also clear that the pre-filmed samples have uniform oxide layer growth. On the other hand, the non-pre-filmed samples have uneven oxide layer growth. These unevenly grown oxides on the surface contributed to a rough surface and increased the interface area between oxide layer and coolant in the test loop.

Table 4.1. Average thicknesses of oxide layers

Time	Pre-filmed samples		Non-pre-filmed samples	
	Average thickness (μm)	Uncertainty (μm)	Average thickness (μm)	Uncertainty (μm)
Original	3.4	0.7	0	0
First month	3.7	1.3	2.6	1.7
Second month	5.2	0.8	5.6	1.9
Third month	5.5	2.8	8.0	3.0
Fourth month	4.4	1.2	7.6	5.8
Fifth month	4.7	1.5	8.5	1.5
Sixth month	3.4	0.8	15.0	5.2

Figure 4.3 shows that there are more deposit spots formed on the rim of the pre-filmed coupon and barely any visible amount of deposits formed on the surface. As a comparison, Figure 4.4 shows deposit distribution on non-pre-filmed coupon from the same month. It's clear that there are more deposit formed on non-pre-filmed coupon. Since the rims of pre-filmed coupons weren't covered by the pre-filmed oxide layer, it could infer that deposits tended to form on non-pre-filmed areas. Then it is reasonable to infer that significant attribution to the formation of the deposit is fast corrosion rate. In fact, the fourth month and fifth month non-pre-filmed coupons showed massive

deposit growth causing serious pitting because a large amount of aluminum alloy was consumed for the deposit formation.

Figure 4.3. Deposit spots distribution on pre-filmed coupon from first month

Figure 4.4. Deposit spots distribution on non-pre-filmed coupon from first month

From the SEM images of samples' cross-sections, compared to the pre-filmed samples, it is clear that non-pre-filmed samples tend to form uneven and thicker oxide layers on the surfaces. Also, non-pre-filmed samples tend to form more deposits, which is a sign

of faster corrosion. More aluminum was being consumed to form deposits from a localized corrosion, which usually leads to pitting as shown in Figure 4.5. Pitting diminishes the mechanical strength of cladding and could lead to fuel release. Faster corrosion and uneven oxide distribution on the surface can form a very thick oxide layer at some spots, as shown in Figure 4.6. These regions would have much lower heat transfer capacity due to the thicker oxide layer.
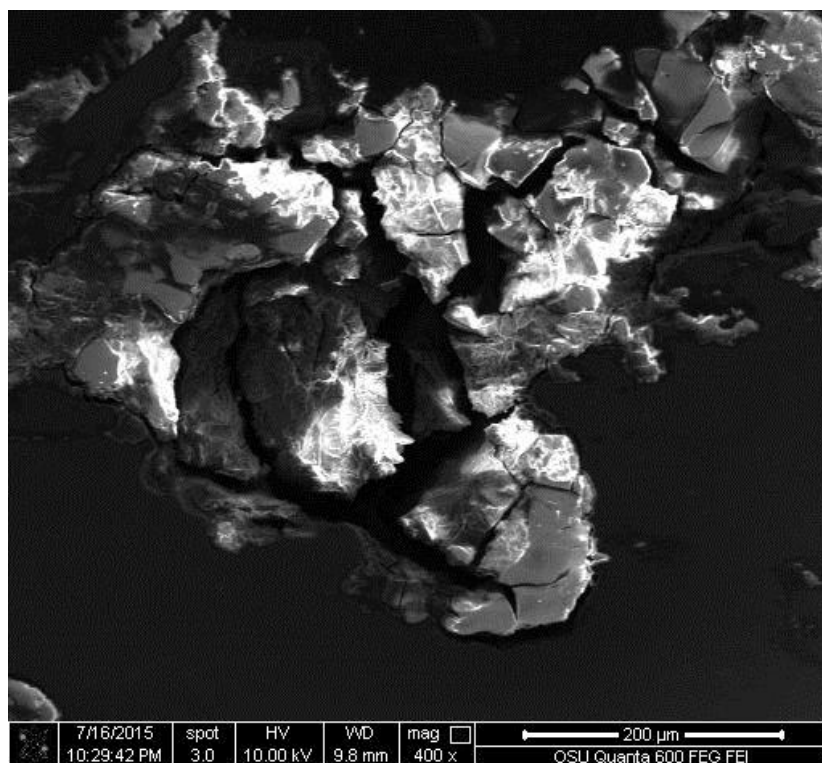
Figure 4.5. Pitting on non-pre-filmed sample from second month

| 7/17/2015 | spot | HV | WD | mag □ | ⊢————— 30 µm —————⊣ |
| 7:31:14 PM | 3.5 | 10.00 kV | 10.5 mm | 3 500 x | OSU Quanta 600 FEG FEI |
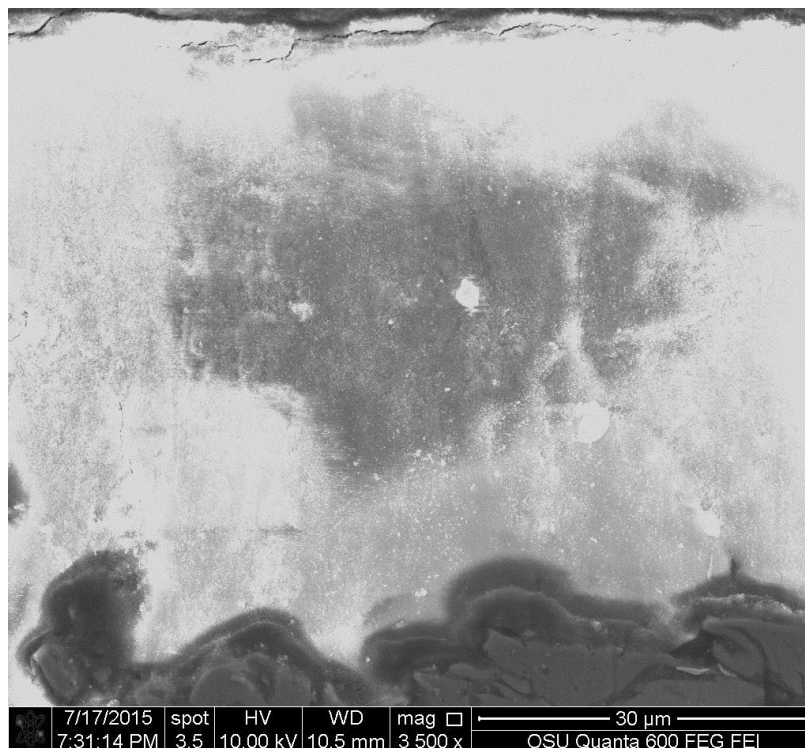
Figure 4.6. Extraordinary oxide layer on a non-pre-filmed coupon from third month

Images of samples' surfaces also show that non-pre-filmed coupon have more prominent corrosion. In Figure 4.7, the surface comparison clearly shows the surface situation. The pre-filmed samples' surfaces are covered by a uniform oxide layer compared to the surface of non-pre-filmed sample. The non-pre-filmed samples' surfaces are covered by an uneven oxide layer. Deposit spots are all over the non-pre-filmed sample from sixth month. Beneath those spots, pits may be present. In comparison, the pre-filmed sample's surface from the sixth month is very flat and clean. A few pits seen in the image might not have been caused by corrosion, but from defects on the original coupon as shown in Figure 4.8. According to this figure, some pits can be clearly seen on the surface of original pre-filmed coupon. These pits may come from fabrication. The original non-pre-filmed coupon, as shown in Figure 4.9, has some scratches and pits on the surface. The average roughness of non-pre-filmed coupon is larger than that of pre-filmed coupon. The higher roughness contributed to the uneven oxide growth on the non-pre-filmed coupons.
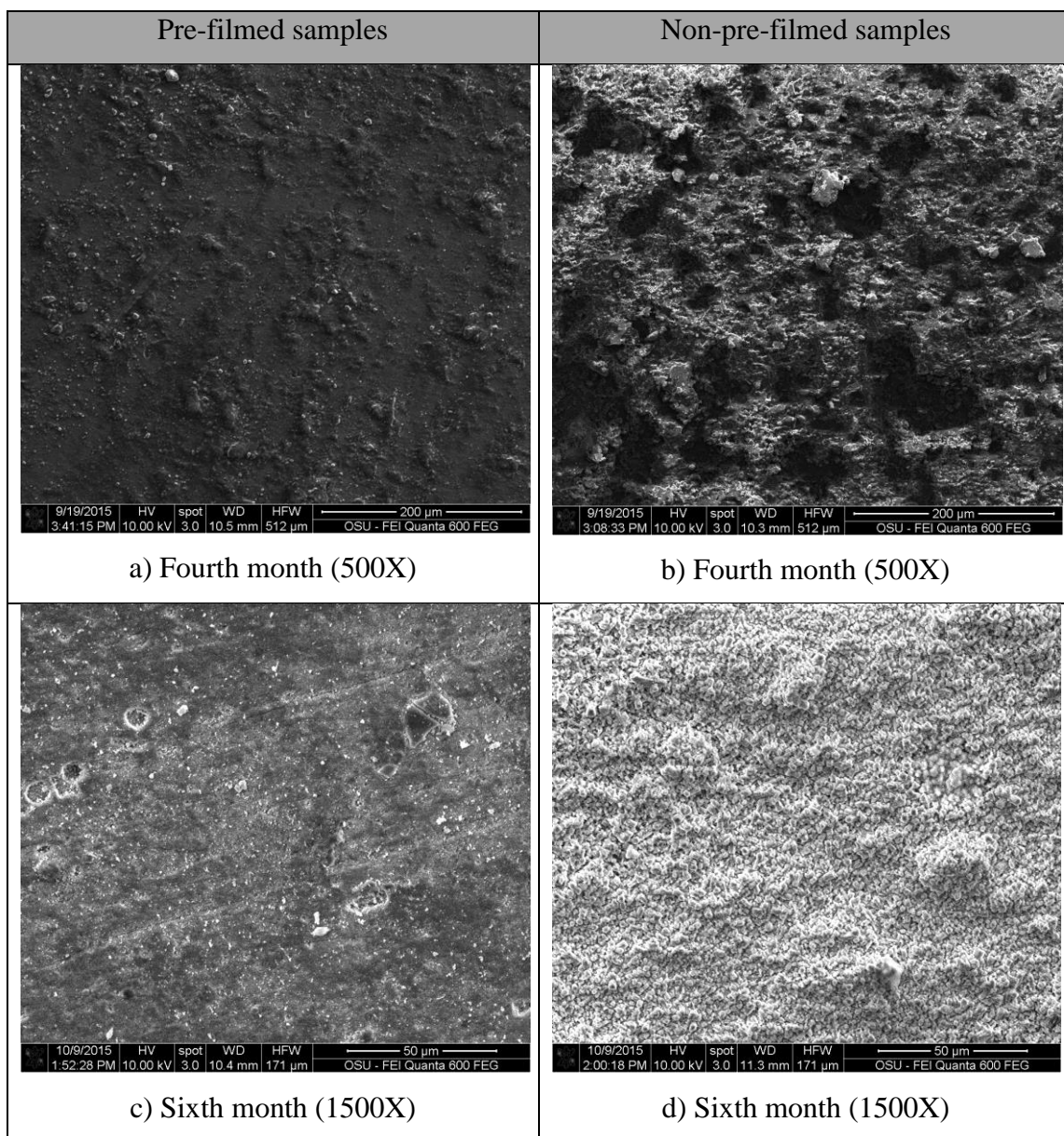
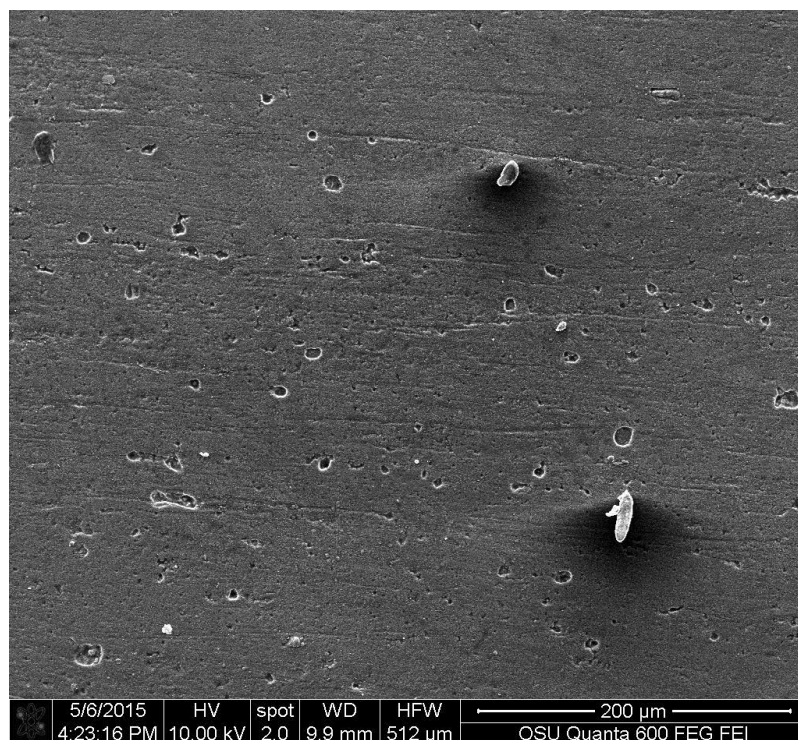| Pre-filmed samples	Non-pre-filmed samples
a) Fourth month (500X)	b) Fourth month (500X)
c) Sixth month (1500X)	d) Sixth month (1500X)

Figure 4.7. Surface comparison

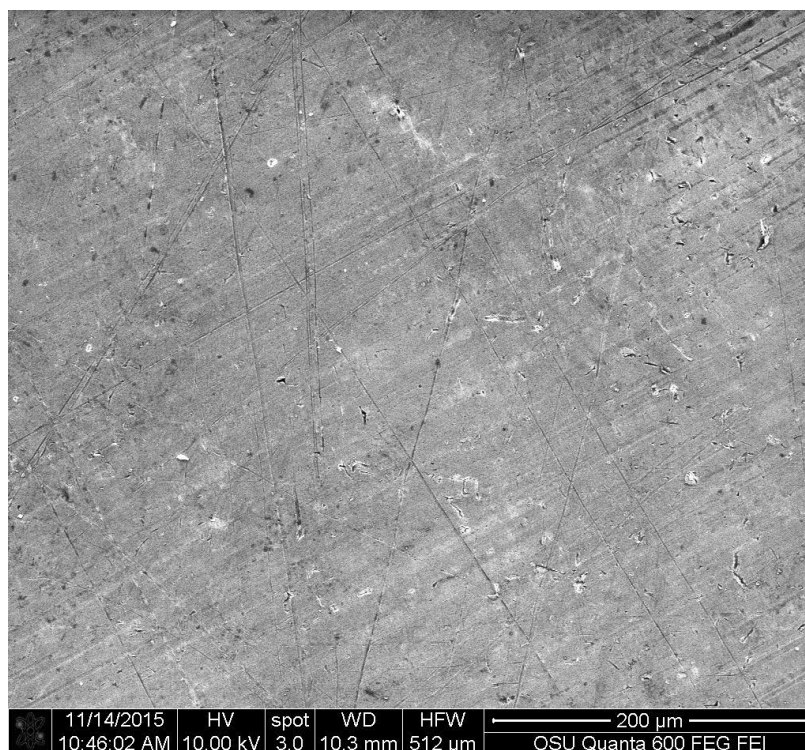Figure 4.8. Surface of original pre-filmed coupons (500X)

Figure 4.9. Surface of original non-pre-filmed coupons (500X)

However, some defects were also observed from pre-filmed samples. Some spots on the pre-filmed coupons were not covered by an intact pre-film as shown in Figure 4.10a, which could lead to a faster corrosion process since the aluminum alloy 6061 had directly contact with coolant. Because of the broken oxide pre-film, irregular oxidation happened, as shown in Figure 4.10b, which could also diminish the alloy's mechanical strength and lead to fuel release. Loose adhesion of oxide layer indicates oxide layer spallation as shown in Figure 4.10c, which could be a reason of having a thin oxide thickness and making weight gain analysis inaccurate.
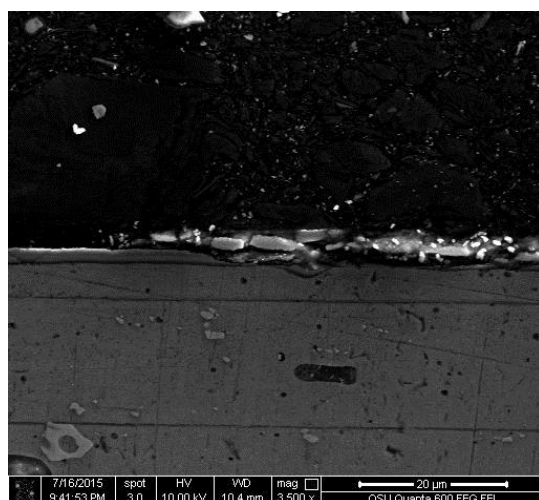
a) Original sample
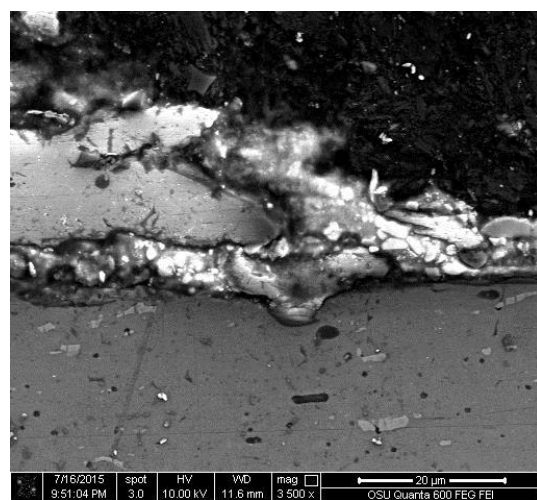
b) First month
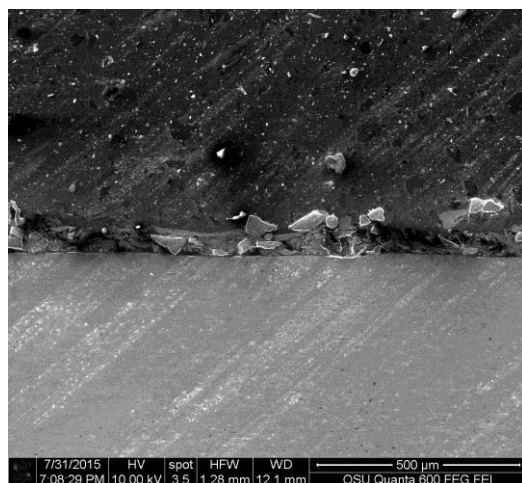
c) Fourth month

Figure 4.10. Defects observed from pre-filmed samples

From the SEM results, the benefits of the pre-film are obvious. It reduces the oxide layer growth rate, which highly reduces the risk of cladding failure or fuel melting due to the heat accumulation caused by thick oxide layers. It helps oxides grow evenly on the surface so that the heat transfer can remain uniform. Pitting is highly restrained by the pre-film layer, so that the aluminum alloy cladding can remain intact and keep its mechanical strength, holding the solid fuel inside. Defects observed on exposed pre-filmed samples are possibly caused by the damage on the original coupon. Those damaged pre-filmed areas were possibly caused during coupon fabrication or material shipping.

4.2   Quantitative analysis of oxide thickness

Based on SEM cross-section images, the average thicknesses of oxides were measured using ImageJ software. The average thicknesses of coupons are shown in Table 4.1 with uncertainty that represent one standard deviation with 68% confidence interval. Using the data recorded from the test loop, the prediction of oxide thicknesses for both types of coupons were calculated using Griess correlation (21), Pawel correlation (22) and Hanson correlation (23).
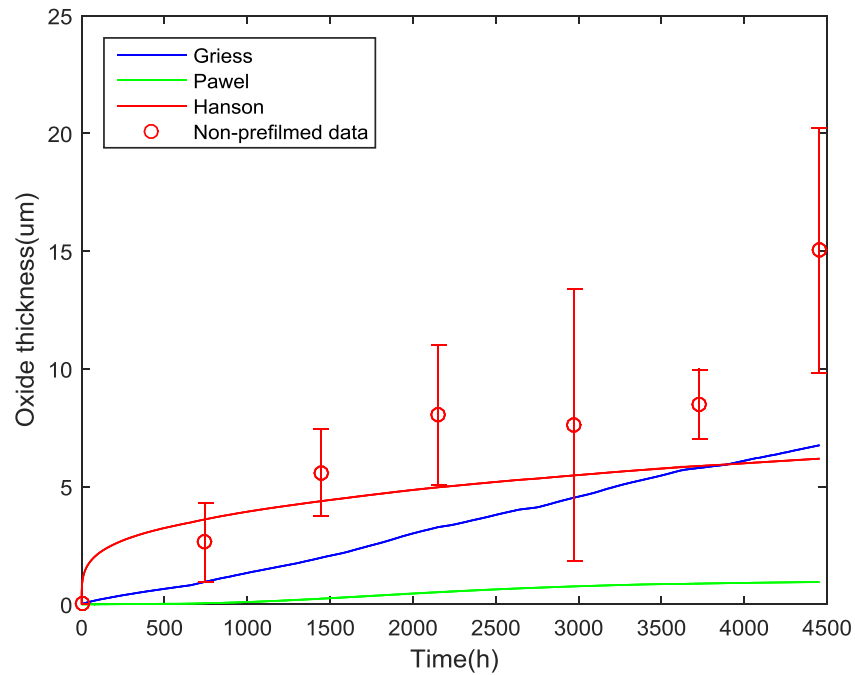
Figure 4.11. Oxide thickness of non-pre-filmed coupons

Figure 4.11 shows the predicted oxide thickness curves with time using Griess, Pawel and Hanson correlations along with the average oxide thickness of non-pre-filmed coupons. According to the plot, it's clear that the average oxide thicknesses on the non-pre-filmed coupons were greater than the predictions of all correlations after 1 month of exposure. The oxide thickness grew significantly in the first month, then the growth rate of oxide decreased in the second month of exposure and stayed at a relatively stable value in the following months. According to the plot, the average oxide thickness of the fourth month decreased. And the oxide thickness for the fifth month almost didn't increase. Possible explanations include:

- Human error involved in the process of taking SEM images

- Stochastic uncertainty

- Breakaway oxidation

The SEM operation and ImageJ analysis followed the given procedures, which should help eliminate the human error. However, the error bars for the fourth month measurement data were very large. In fact, the error bar for the pre-filmed sample from fourth month is the biggest among all months. This suggests that the reason for the thickness decrease for the fourth month may be caused by stochastic uncertainty. Breakaway oxidation is also possible. The trend could be parabolic until a point where the samples start to spall and the oxide layer stops growing in a parabolic trend and gain thickness linearly again. The fourth month sample could have had spallation, which caused the decrease in oxide thickness. A large oxide thickness increase was observed for the sixth month measurement data. The best possible explanation is also stochastic uncertainty and breakaway oxidation.
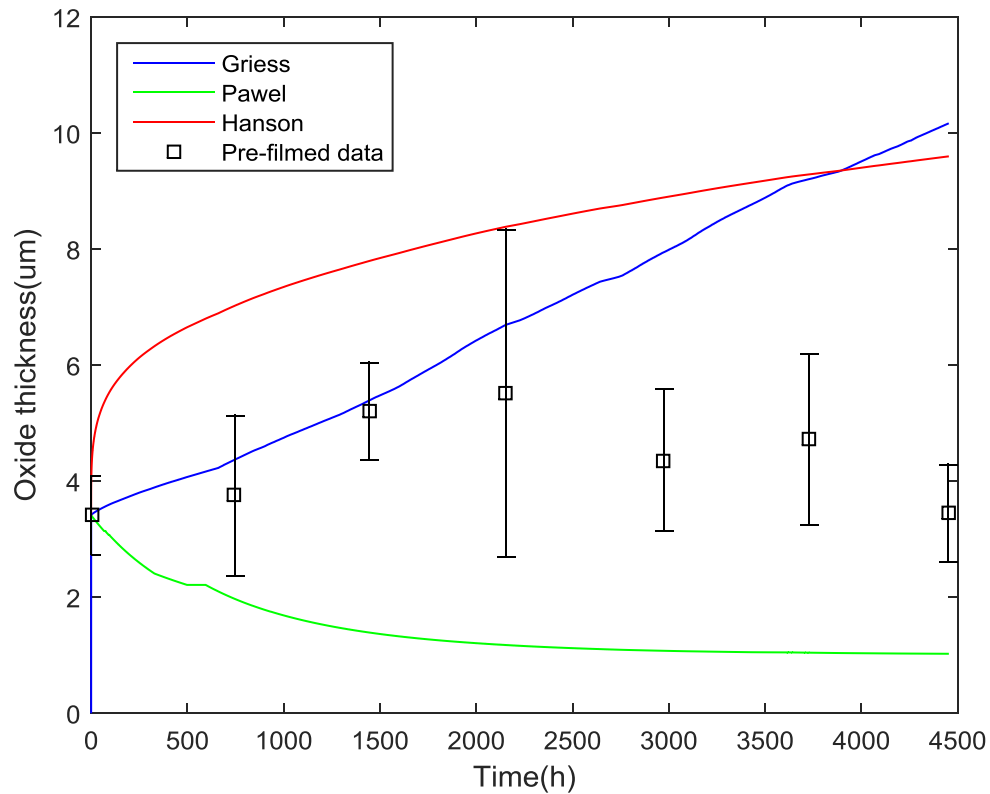

Figure 4.12. Oxide thickness of pre-filmed coupons

Figure 4.12 shows the predicted oxide thickness curves with time using Griess, Pawel and Hanson correlations along with average oxide thickness of pre-filmed coupons.

The initial 2.1μm pre-filmed oxide layer thickness was obtained from ImageJ analysis. The pre-filmed coupon also had a significant oxide growth in the first month of the test. But, as shown in Table 4.1, the pre-filmed sample had a 0.3μm oxide thickness increase in the first month, which is much less than 2.6μm oxide thickness increase for the non-pre-filmed sample. This result reinforced the deduction that the pre-filmed boehmite oxide layer decreases the oxide growth rate. According to the data points in the plot, the average oxide thicknesses from the second and third month were higher than the other data points. However, unlike the third month data point having a large error bar, the second month data's error bar is in a relative normal range. Therefore, the oxide thickness increase in the second month is not due to stochastic uncertainty. During the analysis process, the SEM images for this sample needed to be retaken to match the magnifications with all the others images. So it is possible that error occurring during sample preparation caused the thickness increase. The sixth month measurement data had a decrease in oxide thickness with a small error bar. It's possibly because of the oxide spallation. The reason for this needs further study. The other data points have a relatively stable trend. Comparing the measured oxide thickness data with the oxide thickness prediction, the Griess correlation predicts the first three months measurement data well. The Pawel correlation prediction has negative increases in oxide thickness. It's because the pre-film has a start-up thickness, which is much thicker than the oxide thickness gained each month. And the small power term in the correlation makes the pre-film thickness smaller and leads to a negative thickness increase in total. Therefore, the Pawel correlation couldn't be used on pre-filmed coupons.

Figure 4.13 shows the net change of the average oxide thickness from the measurement data and oxide thickness predictions for both types of coupons. This plot clearly shows that the oxide growth rate of non-pre-filmed coupons is much higher than the pre-filmed coupons.
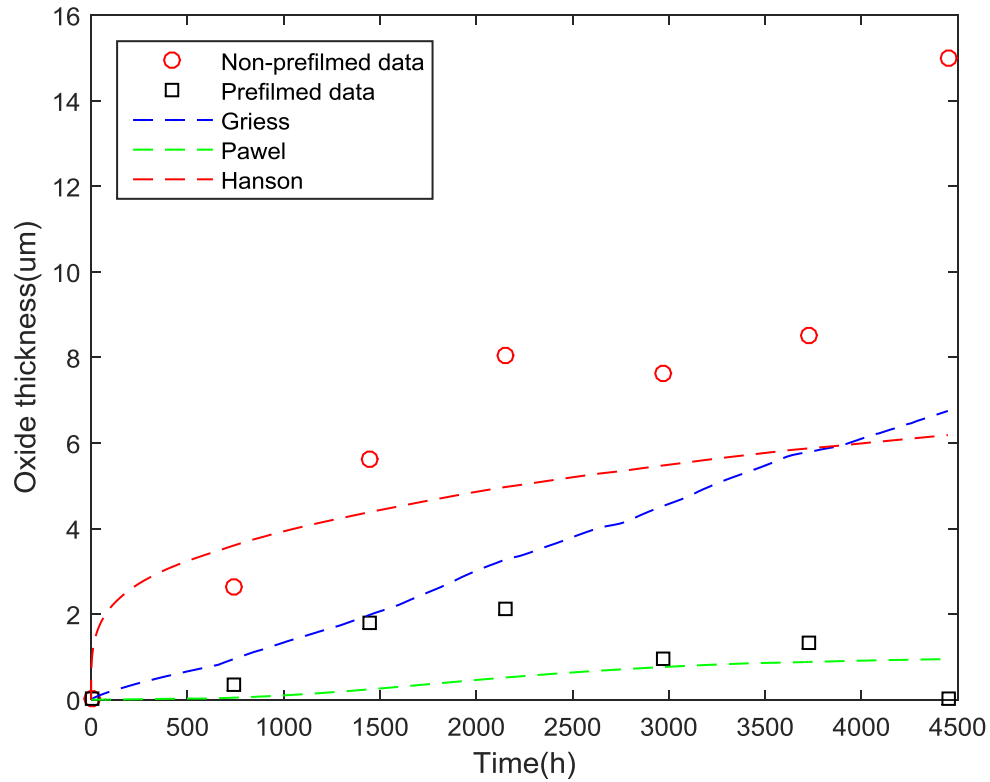
Figure 4.13. Oxide thickness net change of pre-filmed and non-prefilmed samples

Figure 4.14 shows the total oxide thickness for both types of samples. For the pre-filmed samples, the Griess correlation fits the first three months data and then over predicts the oxide thickness for months four through six. Using this correlation would provide additional safety margin in real reactor operation. The Hanson correlation over-predicts oxide thickness for the pre-filmed samples through the entire experiment. But it under estimates the non-pre-filmed samples' oxide thickness for months two through six. Pawel correlation under-predicts the oxide thickness too much for the non-pre-filmed sample. And it provides a negative oxide thickness increase for pre-filmed sample caused by the small power in the correlation.
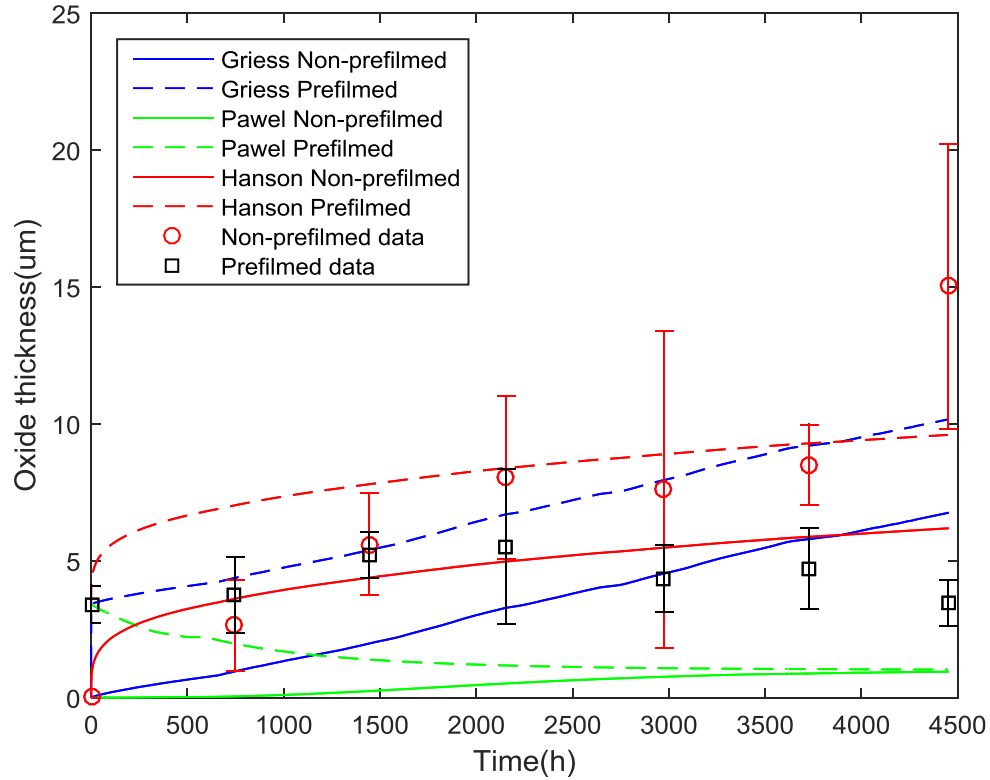
Figure 4.14. All measurement data and prediction curves

While none of the correlations appropriately follow the development of oxide growth on the surface of either sample-sets, the pre-filmed coupons measure smaller oxide thicknesses than that predicted for Hanson and Griess correlations, while the non-pre-filmed coupons measure thicker than any of the correlations predict. This is paramount to the safety of the reactors as correlations are used to support the safety analysis of the reactors that have pre-filmed oxide on cladding. The oxide thickness from safety analyses is thicker than it actually is therefore the state of cladding is conservatively assessed by the Hanson and Griess correlations.

4.3 Chemical analysis results

The chemical formula of boehmite is $AlO(\mathrm{OH})$. The chemical formula of bayerite is $Al(\mathrm{OH})_3$. Bayerite is one of the structural polymorphs of gibbsite, which is one of the mineral forms of aluminum hydroxide. For boehmite, the oxygen weight percentage is

53.3%; the aluminum weight percentage is 45%. For bayerite, the oxygen weight percentage is 34.6%; the aluminum weight percentage is 61.5%. EDS analysis was applied to determine the chemical composition of the deposit and oxide layer. One thing to note is that the standard deviation of the result may be up to 10% for a simple system like oxygen and aluminum. EDS analysis was conducted on the deposits from the first month and fourth month. The reason for doing an analysis for the deposit from first month coupon was because of the cotton-like deposit on the surface was not expected. The chemical composition of deposit needed to be analyzed. The analysis for the fourth month was conducted to compare with the results from first month. According to the first month results, which are shown in Figure 4.15 and Figure 4.16, the aluminum and oxygen percentages from non-pre-filmed coupons are lower than those from the pre-filmed coupons. This is because the result for pre-filmed sample doesn't include the Au and Pd. This leads to an increase in the percentage of the oxygen and aluminum. The presence of Au and Pd from the results is because of the coating process of sample preparation for SEM analysis. The silicon shown in the result was either from the aluminum alloy or from the water in the test loop. Water chemical analysis indicated silica was present. Silicon is also one of the compositional elements of 6061 aluminum alloy, though in much lower concentrations. In all the results, the oxygen percentages were at least 20% higher than the aluminum percentages. In boehmite, the percentage of the oxygen is higher than that of the aluminum. Therefore, the substances of the deposit on both types of coupons were possibly the same (boehmite) or a mixture composed of mainly boehmite with small amount of bayerite.
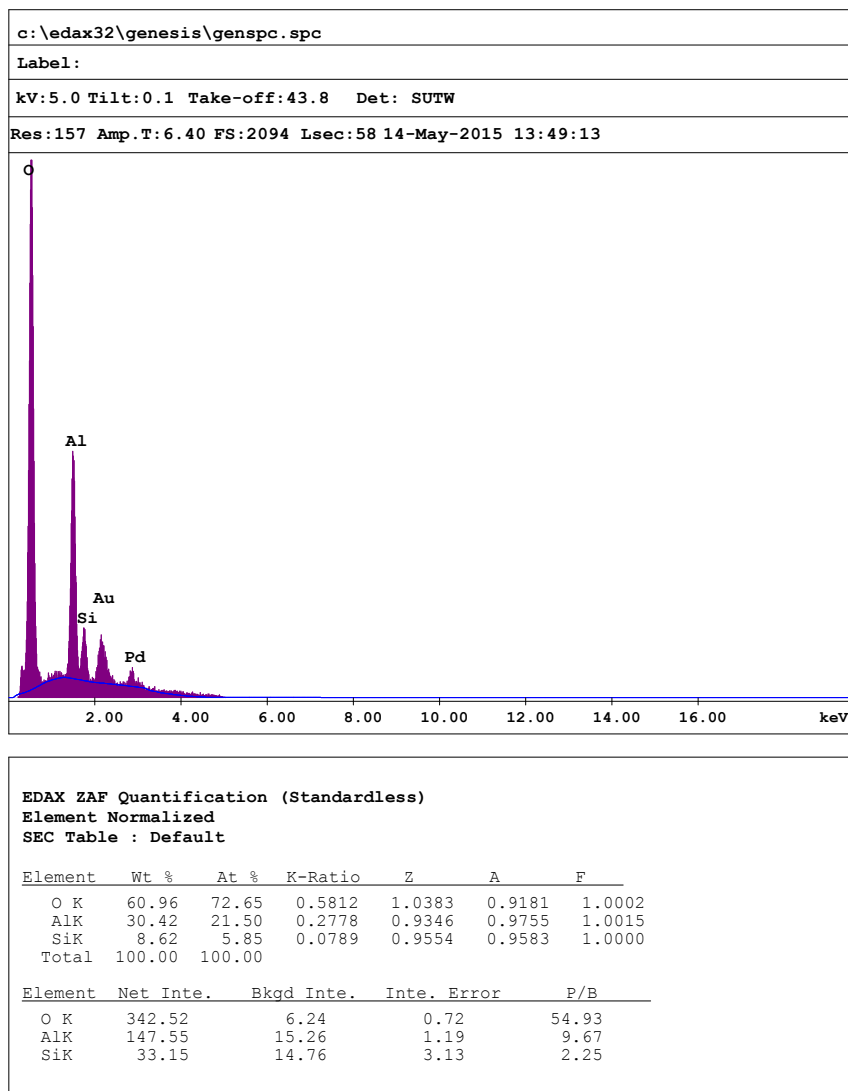
```
c:\edax32\genesis\genspc.spc

Label:

kV:5.0 Tilt:0.1 Take-off:43.8   Det: SUTW

Res:157 Amp.T:6.40 FS:2094 Lsec:58 14-May-2015 13:49:13
```



```
EDAX ZAF Quantification (Standardless)
Element Normalized
SEC Table : Default

Element   Wt %     At %    K-Ratio    Z       A       F
  O K    60.96    72.65    0.5812   1.0383  0.9181  1.0002
  AlK    30.42    21.50    0.2778   0.9346  0.9755  1.0015
  SiK     8.62     5.85    0.0789   0.9554  0.9583  1.0000
 Total  100.00   100.00

Element   Net Inte.    Bkgd Inte.   Inte. Error     P/B
  O K     342.52          6.24         0.72        54.93
  AlK     147.55         15.26         1.19         9.67
  SiK      33.15         14.76         3.13         2.25
```

Figure 4.15. EDS result of deposit formed on pre-filmed sample from first month

```
c:\edax32\genesis\genspc.spc

Label:

kV:5.0 Tilt:0.1 Take-off:43.8   Det: SUTW

Res:157 Amp.T:6.40 FS:738 Lsec:20 14-May-2015 13:56:11
```



```
EDAX ZAF Quantification (Standardless)
Element Normalized
SEC Table : Default

Element   Wt %     At %   K-Ratio    Z        A        F
  O K    42.97    72.25   0.4046   1.1806   0.7976   1.0001
  AlK    17.04    16.99   0.1730   1.0601   0.9567   1.0010
  SiK     3.94     3.77   0.0410   1.0875   0.9574   1.0006
  AuM    18.24     2.49   0.1081   0.5883   1.0074   1.0000
  PdL    17.82     4.50   0.1301   0.7349   0.9939   1.0000
  Total 100.00   100.00

Element   Net Inte.   Bkgd Inte.   Inte. Error     P/B
  O K     336.17        4.83         1.23        69.54
  AlK     129.54       12.81         2.15        10.11
  SiK      24.29       11.91         6.38         2.04
  AuM      25.07        9.97         5.97         2.52
  PdL      10.42        7.33        10.73         1.42
```

Figure 4.16. EDS result of deposit formed on non-pre-filmed sample from first month

EDS analyses were conducted on oxide layers for the samples from the second to fourth month. The results from second month for pre-filmed coupons is shown in Figure 4.17. The analysis had Fe in the result, which couldn't be found in any other EDS results of oxide layers. Since the metal analysis of water indicated that there was Fe element in the water. Therefore the source of Fe could be the alloy itself or from the water. The ratio of oxygen and aluminum percentage indicated that boehmite is the oxide. This deduction was supported by the EDS result from the third month. The

result showed a 54% oxygen and 43% aluminum composition. However, the result had Na presence, shown in Figure 4.17. Since the test loop was using filtered tap water as the coolant, the Corvallis city water quality report was also used as a material to determine what elements were in the water. The results from 2014 water quality report were used here, because (1) the water quality report from 2015 had not come out, (2) the water plants consistently use the same systems and processes so that the water chemical composition barely changed from year to year, (3) by looking at the reports from previous years, it's proved that water chemical composition has been consistent. According the results from 2014 report, the Sodium (Na) content was 20 ppm in the maximum contaminant level. [18] Therefore, a possible source for the sodium was coolant.

```
c:\edax32\genesis\genspc.spc

Label:

kV:5.0 Tilt:0.0 Take-off:43.7   Det: SUTW

Res:181 Amp.T:3.20 FS:620 Lsec:99  5-Jun-2015 14:55:56
```

```
EDAX ZAF Quantification (Standardless)
Element Normalized
SEC Table : Default

Element    Wt %     At %    K-Ratio    Z        A        F

  O K     53.70    67.60    0.5197   1.0558   0.9163   1.0004
  FeL      6.08     2.19    0.0406   0.8024   0.8309   1.0005
  NaK      1.38     1.21    0.0121   0.9674   0.9099   1.0026
  AlK     38.84    29.00    0.3582   0.9501   0.9705   1.0000
  Total  100.00   100.00

Element   Net Inte.    Bkgd Inte.    Inte. Error     P/B

  O K      70.03         1.58          1.22        44.23
  FeL       1.69         2.65         15.62         0.64
  NaK       1.90         3.13         15.02         0.61
  AlK      43.51         2.40          1.60        18.17
```

Figure 4.17. EDS result of oxide layer on pre-filmed coupon from second month

```
c:\edax32\genesis\genspc.spc

Label:

kV:5.0 Tilt:0.0 Take-off:45.0   Det: SUTW

Res:222 Amp.T:1.60 FS:2770 Lsec:135  1-Jul-2015 14:37:19
```

O

Al

Na   Si

| 1.00 | 2.00 | 3.00 | 4.00 | 5.00 | 6.00 | 7.00 | 8.00 | keV |

```
EDAX ZAF Quantification (Standardless)
Element Normalized
SEC Table : Default

Element   Wt %    At %   K-Ratio   Z       A       F
  O K    54.08   66.31   0.5183   1.0473  0.9149  1.0003
  NaK     2.46    2.10   0.0220   0.9598  0.9268  1.0033
  AlK    43.46   31.59   0.3999   0.9425  0.9764  1.0000
  SiK     0.00    0.00   0.0000   0.9636  0.9472  1.0000
 Total  100.00  100.00

Element   Net Inte.   Bkgd Inte.   Inte. Error    P/B
  O K    128.59         5.04         0.79        25.49
  NaK      6.33        12.42         7.58         0.51
  AlK     89.37        11.23         1.02         7.96
  SiK      0.00         9.51         0.00         0.00
```

Figure 4.18. EDS result of oxide layer on pre-filmed coupon from third month
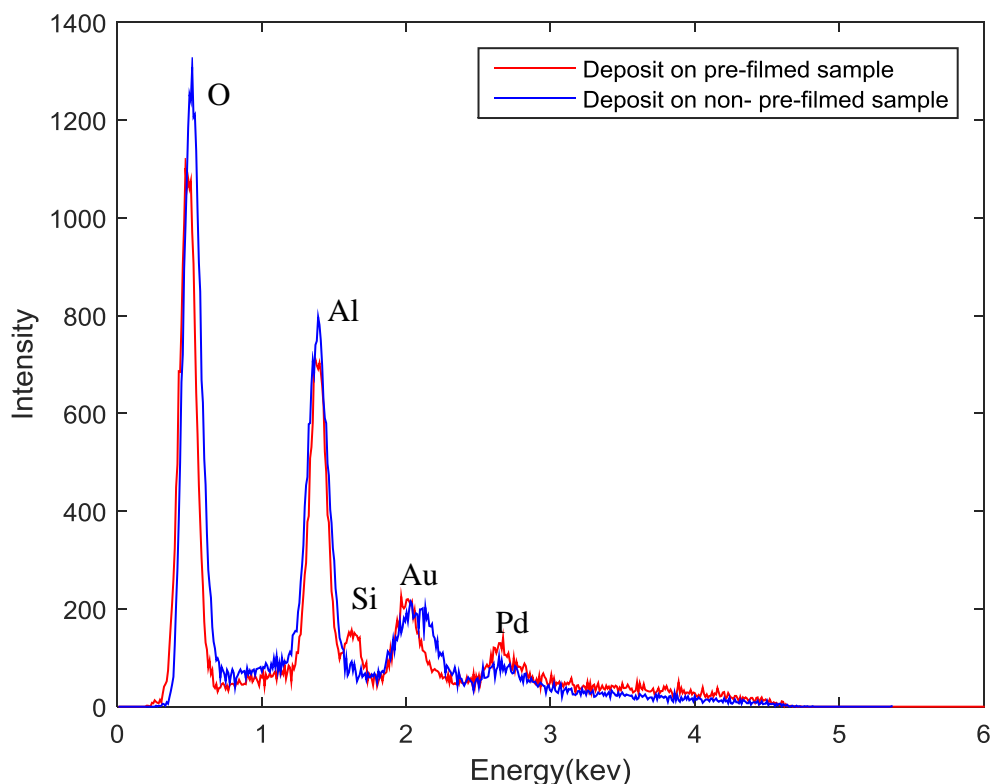
Figure 4.19. Deposit from both type of coupons from fourth month

Figure 4.19 shows deposit EDS results comparison from the fourth month. The red spectrum represents deposit of pre-filmed sample and the blue spectrum represents deposit of non-pre-filmed sample. The trends of these two spectrums are similar and don't have a significant change compared to the deposit spectrum from first month. This again indicates the chemical compositions of deposits are the same on both type of samples.

4.4 Phase identification results

The XRD analysis was conducted on six samples. X-rays were used to scan the sample's surface where the oxide layer formed. XRD analysis was first conducted on the original pre-filmed sample to characterize it. The results are shown in Figure 4.20. The peaks marked with blue are in accordance with peaks of the face-centered cubic aluminum structure. Those peaks have strong intensity, which is reasonable since

aluminum alloy was just beneath the oxide layer that was being scanned. Any surface defect such as cracking and pitting would expose the aluminum alloy to the X-ray and lead to strong intensity peaks for aluminum in the result. Also, other substance peaks may appear at the same position, which increases the intensity and enhances the height of those peaks. The peaks marked with green are in accordance with peaks of boehmite. These peaks cover most of the secondary peaks in the results indicating that the substance composed oxide layer probably is boehmite. Some peaks of boehmite appear at the same position of aluminum's peak, so that these peaks are contributing to the high peaks for the aluminum. After peaks of aluminum and boehmite are identified, there are still a few small peaks left unidentified. The black and purple marks represented gibbsite with different crystal structures. However, among all the marks for gibbsite structure, only a small portion of these marks that are showing in the figure located at unidentified peaks. Therefore, a small amount of gibbsite could be found in the sample.
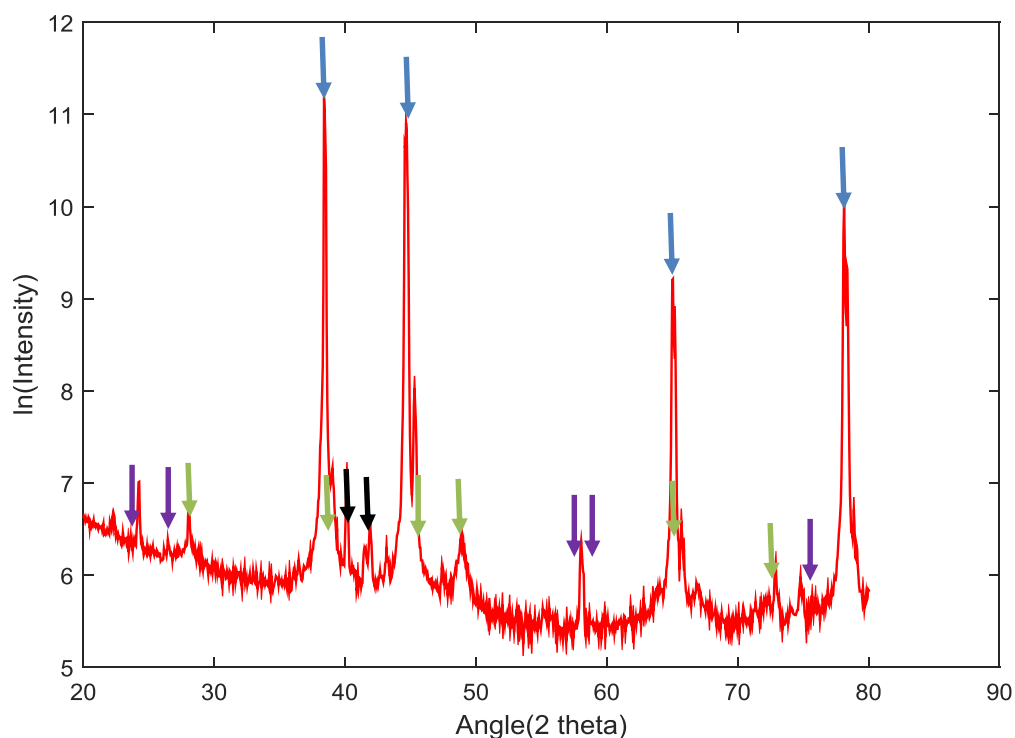
Figure 4.20. XRD results for the original pre-filmed sample

Figure 4.21 shows XRD results of the pre-filmed sample from third month. The peaks marked with blue are in accordance with peaks of aluminum. The peaks marked with green are in accordance with peaks of boehmite. Green marked peaks covered most of the secondary peaks in the results. It is believed that those secondary peaks are the XRD results for the oxide layer. As mentioned above, there are two reasons that those highest peaks indicated aluminum not the oxide layer. Therefore, the secondary peaks most likely are the peaks of interest, which are the peaks of oxide layer. So it is reasonable to infer that boehmite is the potential substance that composed the oxide layer on the pre-filmed sample from third month. Peaks marked with purple are in accordance with boehmite ($Al_2O_3 \cdot H_2O$). And the peaks marked with black are in accordance with peaks of gibbsite. Therefore, the gibbsite and boehmite possibly exist in the sample.
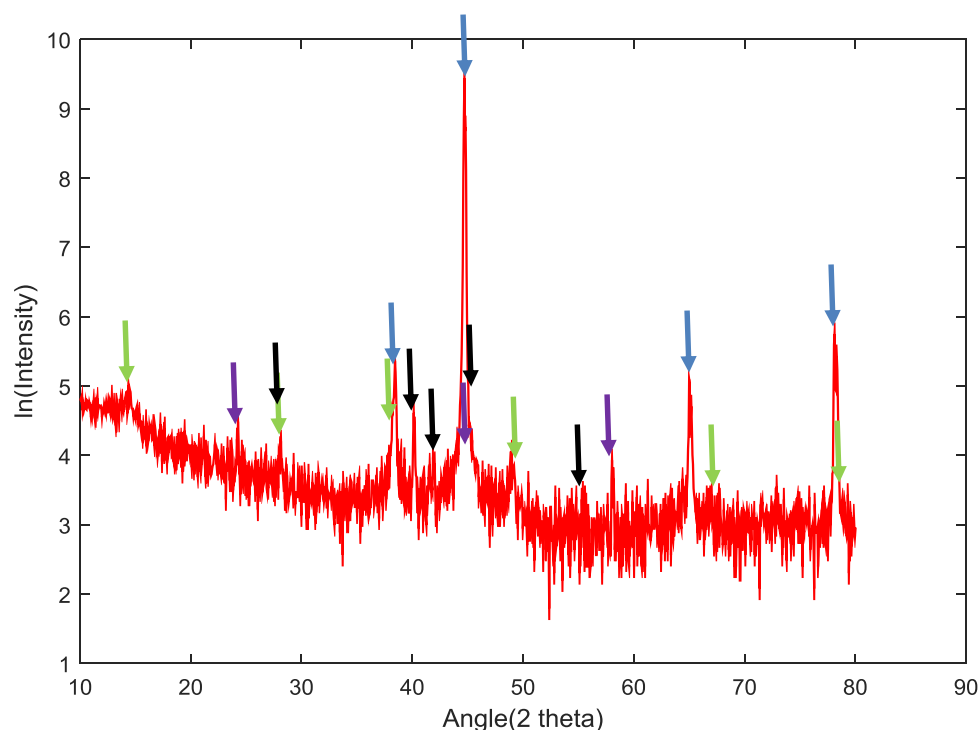
Figure 4.21. XRD results of pre-filmed sample from third month

In Figure 4.22, the peaks marked with blue are in accordance with peaks of aluminum. The secondary peaks marked with green are in accordance with peaks of boehmite. Therefore, the potential substance composed the oxide layer is also boehmite for the non-pre-filmed sample from third month. The peaks marked with black are in accordance with the peaks of gibbsite. The peaks marked with purple are in accordance with the peaks of aluminum hydroxide.
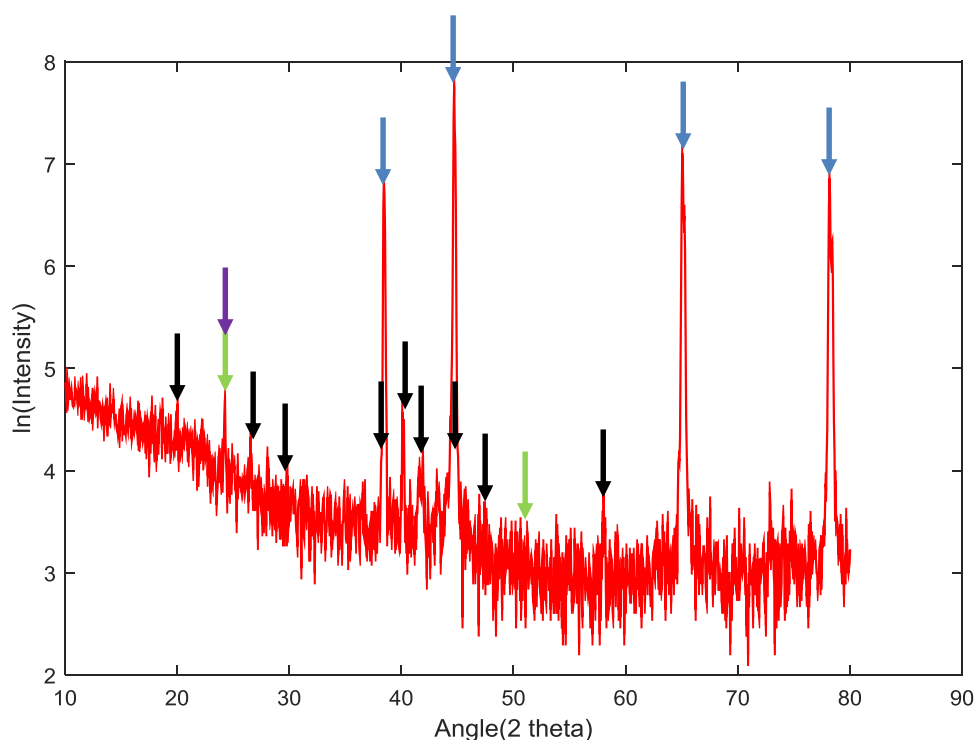
Figure 4.22. XRD results of non-pre-filmed sample from third month

The XRD analysis results for the pre-filmed and non-pre-filmed samples from fourth month are showed in Figure 4.23 and Figure 4.24, respectively. In Figure 4.23, the peaks marked with blue are in accordance with the peaks of aluminum. The peaks marked with green and black are in accordance with the peaks of boehmite with different crystal structures. As it is shown in the figure, the boehmite peaks fit most of the obvious peaks in the result, which indicates that the oxide layer is composed of boehmite. A few small peaks are not identifiable. The reason for this is possibly because of the excessive background reducing, which is one of the operations to

analyze the X-ray scan results. Since the peaks are similar to those from previous results, the potential substance that provides those peaks is possibly gibbsite.
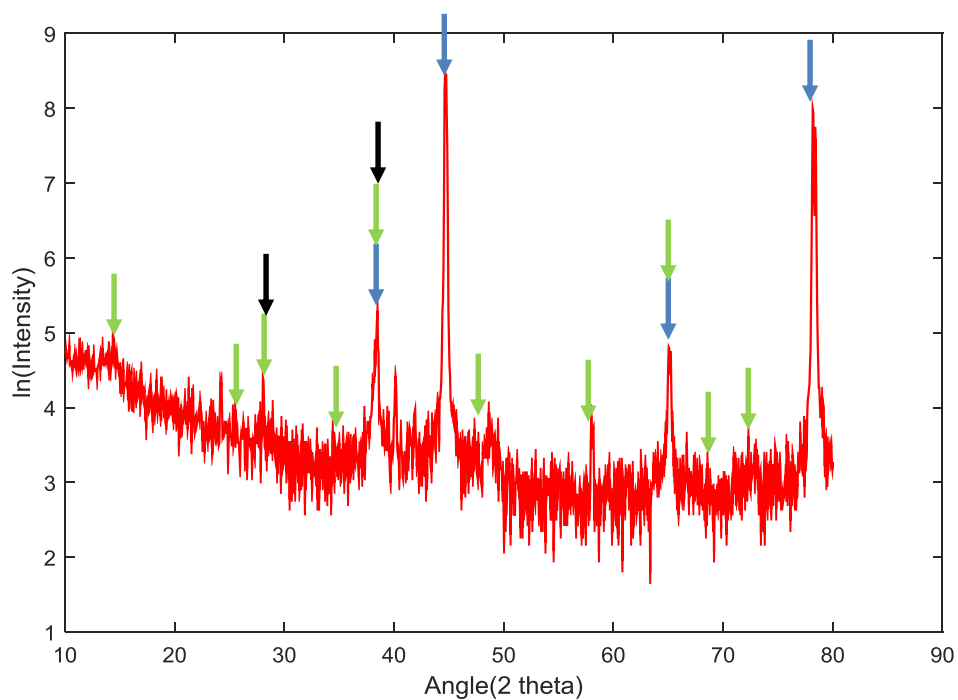
Figure 4.23. XRD results for the pre-filmed sample from fourth month

In Figure 4.24, most of peaks are covered by peaks of boehmite. Therefore, the substance that composes the oxide layer could be inferred as boehmite for the non-pre-filmed sample from fourth month.
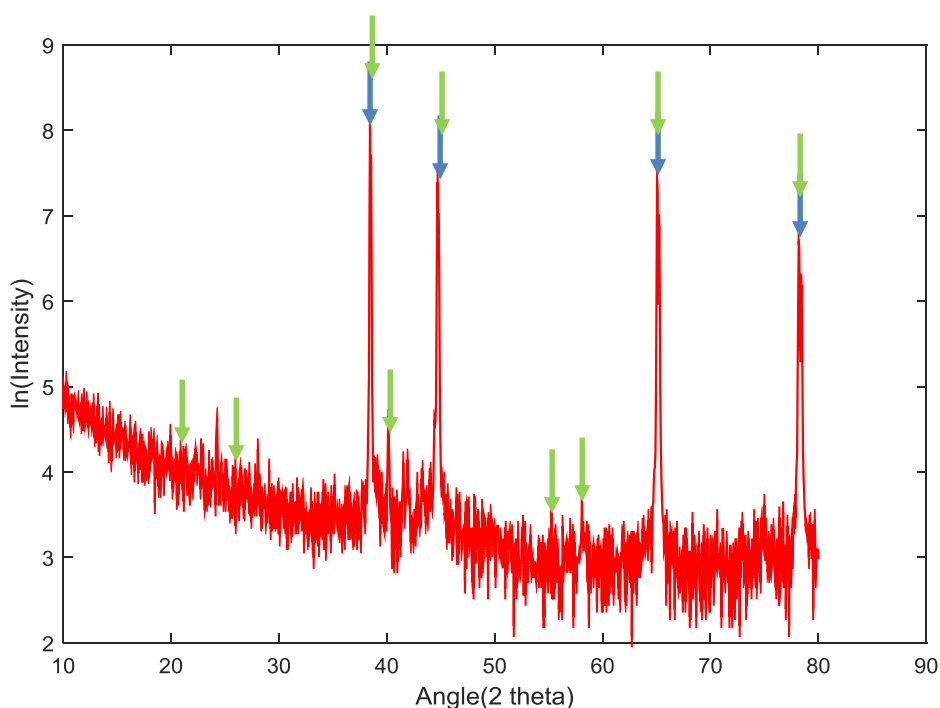
Figure 4.24. XRD results for the non-pre-filmed sample from fourth month

Based on all the peak images, a similar peak pattern is observed from all the XRD analysis. The results have shown that the detected substances are mainly aluminum and boehmite. A few results show some weak peaks indicating the existence of gibbsite. Therefore, under these test conditions, the corrosion products of two different types of samples are essentially the same substance, which is boehmite.

4.5   Supplemental results

The results of weight gains of coupons extracted from each month are shown in Figure 4.25. Each sample was measured three times. The average values are shown in that figure. The standard deviation for each data point is many orders of magnitude smaller than the average value, so that can be ignored. The result shows that pre-filmed coupons' weight keep increasing through the entire experiment except data points from the sixth month. The rate of weight gain isn't stable. The most significant weight gain in one month occurred in third month. Yet there is no evidence from the data of oxide thickness supporting this significant weight gain. However, the most negative

weight gain (weight loss) from sixth month is in accordance with the decreasing in oxide thickness of pre-filmed sample from sixth month. Weight change data from other months is not in accordance with the change of oxide thickness change. The weight change, specifically weight gain analysis, is not providing useful data for pre-filmed samples.

For the non-pre-filmed coupons, no clear increasing trend of weight changing is shown in the figure. The data is sporadically distributed on the plot. Weight gain for the third and fourth months are smaller than that from second month. The weight gain from the fifth month even has a negative value. The unstable weight change may be caused by the prominent corrosion process happening on non-pre-filmed coupons. As discussed before, more deposits formed on the non-pre-filmed coupon's surface. A noticeable amount of deposit was also lost during the sample collecting process. The amount of oxide product lost in the test loop was small, since the flow rate was very low in the test loop.

Therefore, the weight gain analysis is unreliable for corrosion analysis as the corrosion product loss is very difficult to avoid through the experiment process. Corrosion product could be lost during the corrosion test, coupon collecting process and unexpected accidents through measuring process. Those uncontrollable and unexpected weight loss make weight gain analysis too inaccurate to provide reliable data for this study.
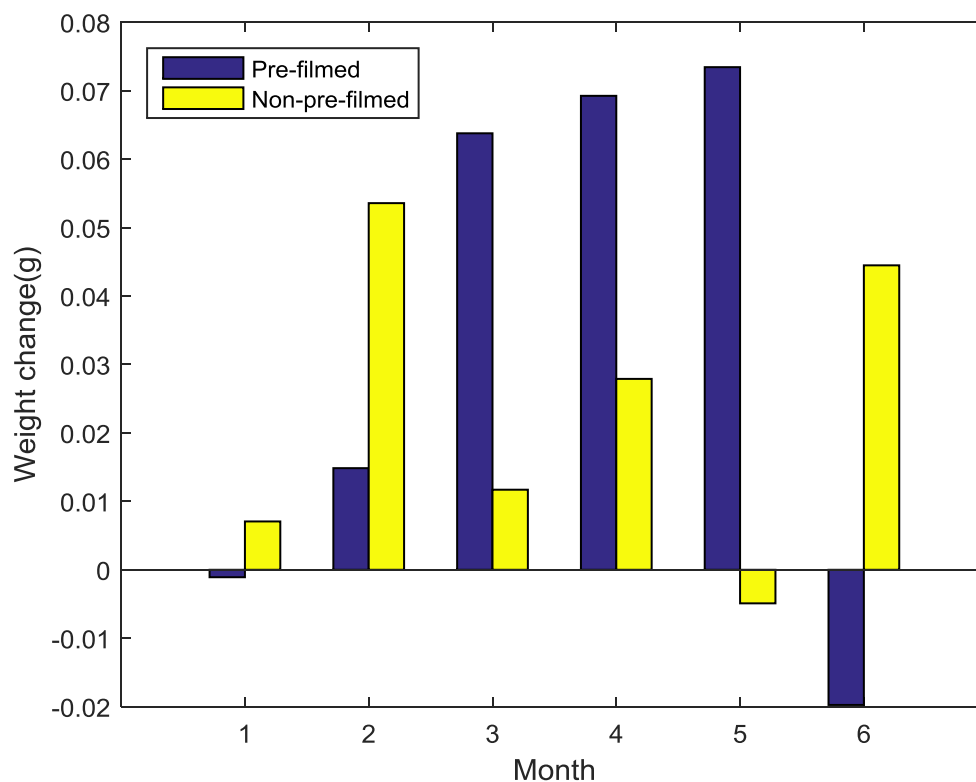
Figure 4.25. Coupons' weight changes

5   CONCLUSION

The objective of this project were as follows:

(1) Extend existing database for the corrosion of aluminum alloys

(2) Evaluate the existing correlations for the new experimental conditions

(3) Help increase the research reactors' operation safety confidence

(4) Evaluate the necessity of the pre-filmed boehmite layer.

An experimental test loop was designed to provide low pressure and temperature conditions for the corrosion tests. The test conditions that were recorded by the test loop are as follows:

- Temperature
- Pressure

- pH
- Exposure time
- Conductivity

Pre-filmed coupons and non-pre-filmed coupons were exposed inside the test loop. During the six months experiment time, one or two coupons of each type were extracted from test loop each month for post exposure analysis. The oxide thicknesses of coupons were measured by analyzing the SEM images using ImageJ and Matlab script. The corrosion database for aluminum alloy 6061 was extended by testing under new conditions. The temperature and exposure time data, recorded by test loop, were plugged into existing correlations (Griess, Pawel and Hanson correlations) to predict the oxide thickness. The predicted oxide thicknesses and measured oxide thicknesses were compared to evaluate the existing correlations. None of the existing correlations predicted the oxide thickness precisely under the low pressure and low temperature conditions for both sample-sets. The oxide thicknesses on the pre-filmed coupons were thinner than prediction, while the oxide thicknesses on the non-pre-filmed coupons were thicker than prediction. This is paramount to the safety of reactors since the correlations are used to support the safety analysis on pre-filmed cladding in NRTR. Therefore, based on 6 months of data, the oxide thickness is assessed conservatively as the oxide thickness from the Griess and Hanson correlations is predicted to be thicker. Based on the significantly larger oxide thicknesses on non-pre-filmed samples and evidence of excessive corrosion on non-pre-filmed coupons from SEM images, the pre-filmed boehmite layer is necessary for the cladding in NRTR.

Future work for this project should be focused on collecting more data in order to ensure the increasing trend of oxide thickness and develop a new correlation or modify the existing correlations to improve oxide thickness predictions. Since the boehmite is the primary substance composing the oxide layer, then the heat conductivity of the oxide layer is known. Therefore, the maximum oxide layer thickness to run a nuclear research and test reactor under these project conditions can be determined. Weight change analysis, especially the weight gain analysis, is unreliable for corrosion tests

because of the corrosion product loss during the corrosion process, coupon collecting process and unexpected accidents during measuring process. Those unavoidable and unexpected weight loss make weight gain analysis too inaccurate to provide any useful information for the study. New analysis techniques would need to be implemented for future studies. Weight gain is considered standard for high temperature gaseous corrosion while weight loss is considered standard for aqueous corrosion.

6   NOMENCLATURE

SEM   -Scanning electron microscope

EDS   -Energy Dispersive Spectroscopy

XRD   -X-ray diffraction

NRTR   -Nuclear Research and Test Reactors

HFIR   -High Flux Isotope Reactor

ATR   -Advanced Test Reactor

ANS   -Advanced Neutron Source

x -oxide thickness

ε -25.4, convertion factor

θ -time

K -surface temperature

a   -constant, equals 443 at pH $= 5$

b -constant, equals 0.778 at pH $= 5$

p -constant, equals 4600 at pH $= 5$

n -constant

T_c -local coolant temperature

q -local heat flux

x_θ -film thickness at time θ

x_0 -film thickness at time 0 (θ_0)

k -rate constant

R -oxide surface temperature

q -heat flux

HFW   -horizontal field width

DT   -dead time

CPS   -counts per seconds

x_i -total oxide thickness at $Time_{(i)}$

$x_{(i-1)}$ -total oxide thickness at $Time_{(i-1)}$

$Time_{(i)}$ -total exposure time at i^{th} data point

7   REFERENCES

1.   Griess, J., et al., *Effect of Heat Flux on the Corrosion of Aluminum by Water. Part I. Experimental Equipment and Preliminary Test Results*. 1960, Oak Ridge National Lab., Tenn.
2.   Griess, J., et al., *Effect of Heat Flux on the Corrosion of Aluminum by Water. Part II. Influence of Water Temperature, Velocity, and pH on Corrosion-Product Formation*. 1961, Oak Ridge National Lab., Tenn.
3.   Griess, J., et al., *Effect of Heat Flux on the Corrosion of Aluminum by Water. Part III. Final Report on Tests Relative to the High-Flux Isotope Reactor*. 1961, Oak Ridge National Lab., Tenn.
4.   Griess, J., H. Savage, and J. English, *EFFECT OF HEAT FLUX ON THE CORROSION OF ALUMINUM BY WATER. PART IV. TESTS RELATIVE TO THE ADVANCED TEST REACTOR AND CORRELATlON WITH PREVIOUS RESULTS*. 1964.
5.   Pawel, R., et al., *The development of a preliminary correlation of data on oxide growth on 6061 aluminum under ANS thermal-hydraulic conditions*. 1990, Oak Ridge National Lab., TN (United States).
6.   Pawel, S., D. Felde, and R. Pawel, *Influence of coolant pH on corrosion of 6061 aluminum under reactor heat transfer conditions*. 1995, Oak Ridge National Lab., TN (United States).
7.   Kim, Y.S., et al. *Prediction Model for Oxide Thickness on Aluminium Alloy Cladding During Irradiation*. in *25th Int. Meeting on RERTR, Chicago, IL*. 2003.
8.   Davis, J.R., *Corrosion of aluminum and aluminum alloys*. 1999: Asm International.
9.   Petrovic, J. and G. Thomas, *Reaction of aluminum with water to produce hydrogen.* US Department of Energy, 2008.
10.   Wefers, K. and C. Misra, *Oxides and hydroxides of aluminum.* 1987.
11.   Shaber, E. and G. Hofman, *Corrosion Minimization for Research Reactor Fuel.* Idaho National Laboratory Report INL/EXT-05-00256, 2005.
12.   Badawy, W., F. Al-Kharafi, and A. El-Azab, *Electrochemical behaviour and corrosion inhibition of Al, Al-6061 and Al–Cu in neutral aqueous solutions.* Corrosion Science, 1999. **41**(4): p. 709-727.
13.   El-Menshawy, K., et al., *Effect of aging time at low aging temperatures on the corrosion of aluminum alloy 6061*. Corrosion science, 2012. **54**: p. 167-173.
14.   Sindelar, R.L., G.T. Chandler, and J.L. Micalonis, *Water quality and corrosion: considerations for nuclear reactor systems.* Journal of the South Carolina Academy of Science, 2011. **9**(1): p. 13.
15.   Hanson, G., et al., *ATR-ETR rates of oxide film formation on aluminum fuel plates*. 1974, Aerojet Nuclear Co., Idaho Falls, ID.
16.   Ondrejcin, R., *Evaluation of Mark 22 cladding*. 1983, Du Pont de Nemours (EI) and Co., Aiken, SC (USA). Savannah River Lab.

17. *Aluminium Alloy 6061 - Composition, Properties, Temper and Applications of 6061 Aluminium.* 2015; Available from: http://www.azom.com/article.aspx?ArticleID=3328.

18. *City of Corvallis, OR : Water Quality.* 2015 [cited 2015 October 12th]; Available from: http://www.corvallisoregon.gov/index.aspx?page=998.

8   APPENDIX A – SAMPLE PROCEDURES AND LABELING

Sample procedure

1. Gloves were used for handling the samples to avoid bodily contamination.
2. Put original coupons into box. Coupons are physically isolated from each other to prevent the damage caused by physical contact.
3. Dry coupons by putting them into the boxes with desiccant inside for 7 days.
4. Weigh the original coupons to get original samples weight.

    4.1 Label the coupons with identification numbers.

    4.2 Label the trays with corresponding identification numbers.

    4.3 Weight each tray three times and take average value as the weight of each tray

    4.4 Using a lab notebook to record all the data.

    4.5 Put the sample onto corresponding tray and weight three times for each. Take the average value as the weigh for each tray plus coupon.

5. Take one of each type of coupons out of the experimental test loop every month for the examination.
6. Take coupons off the train and put the each wet coupon into individual plastic sealed bag.
7. Dry coupons by putting them into the boxes with desiccant inside for 7 days.
8. Weight the coupons using the same procedure indicated in 4.5.
9. Clean the deposit from coupon surface and storage deposit in case for future analysis need.
10. Weight the coupon again without deposit.
11. Sample preparation for SEM

    11.1   For coupons taken out of the loop, cut a part off from the coupon and mount it into a sample with the cross-section revealing on the sample surface.

    11.2   The rest of the coupon will be directly mounted in the SEM with no pre-preparation.

12. SEM examination

12.1   Taking picture of samples with various magnification. (magnification can be changed depending on actual situation.)

12.2   Objective of the pictures are thickness of the oxide layer and the surface of the aluminum alloy, looking for the cracks and pitting.

13. Using EDS to learn about the chemistry as a function of oxide depth.

14. XRD examination.

15. After examination, put samples back into the same storage. Air isolated for future use.

Sample preparation procedure for SEM analysis

1. After sample is dried, the sample is cut by a low speed saw using diamond blade and cutting oil.

2. Cutting route is selected by the rule, which is avoiding as many deposits locations as possible. So that the cross-section can provide normal oxide thickness.

3. The sample is cleaned by soap water and ethyl alcohol and dried by compressed air.

4. The cross-section sample is mounted in bakelite with cross-section facing up on the mount surface.

5. The mounted sample is grinded on sandpaper with 240, 320, 400 and 600 grits, respectively, to smooth the surface and remove the damaged part from cutting process.

6. Then sample is polished using progressively fine solutions composed of alumina particles of 5 µm, 0.3 µm, and 0.05 µm in diameters, respectively, on polishing wheels.

7. Sample is cleaned using water before moving to the next wheel to ensure the polishing quality.

8. Polished sample is cleaned by water and dried with compressed air.

Table 8.1. Coupon labeling

Non pre-filmed coupon		Pre-filmed coupon	
Sample #	ID #	Sample #	ID#
1	N-01	1	B-01
2	N-02	2	B-02
3	N-03	3	B-03
4	N-04	4	B-04
5	N-05	5	B-05
6	N-06	6	B-06
7	N-07	7	B-07
8	N-08	8	B-08
9	N-09	9	B-09
10	N-10	10	B-10
11	N-11	11	B-11
12	N-12	12	B-12
13	N-13	13	B-13
14	N-14	14	B-14
15	N-15	15	B-15
16	N-16	16	B-16
17	N-17	17	B-17
18	N-18	18	B-18
19	N-19	19	B-19
20	N-20	20	B-20
21	N-21	21	B-21
22	N-22	N/A	N/A
23	N-23	N/A	N/A
24	N-24	N/A	N/A

9   APPENDIX B – SEM IMAGES
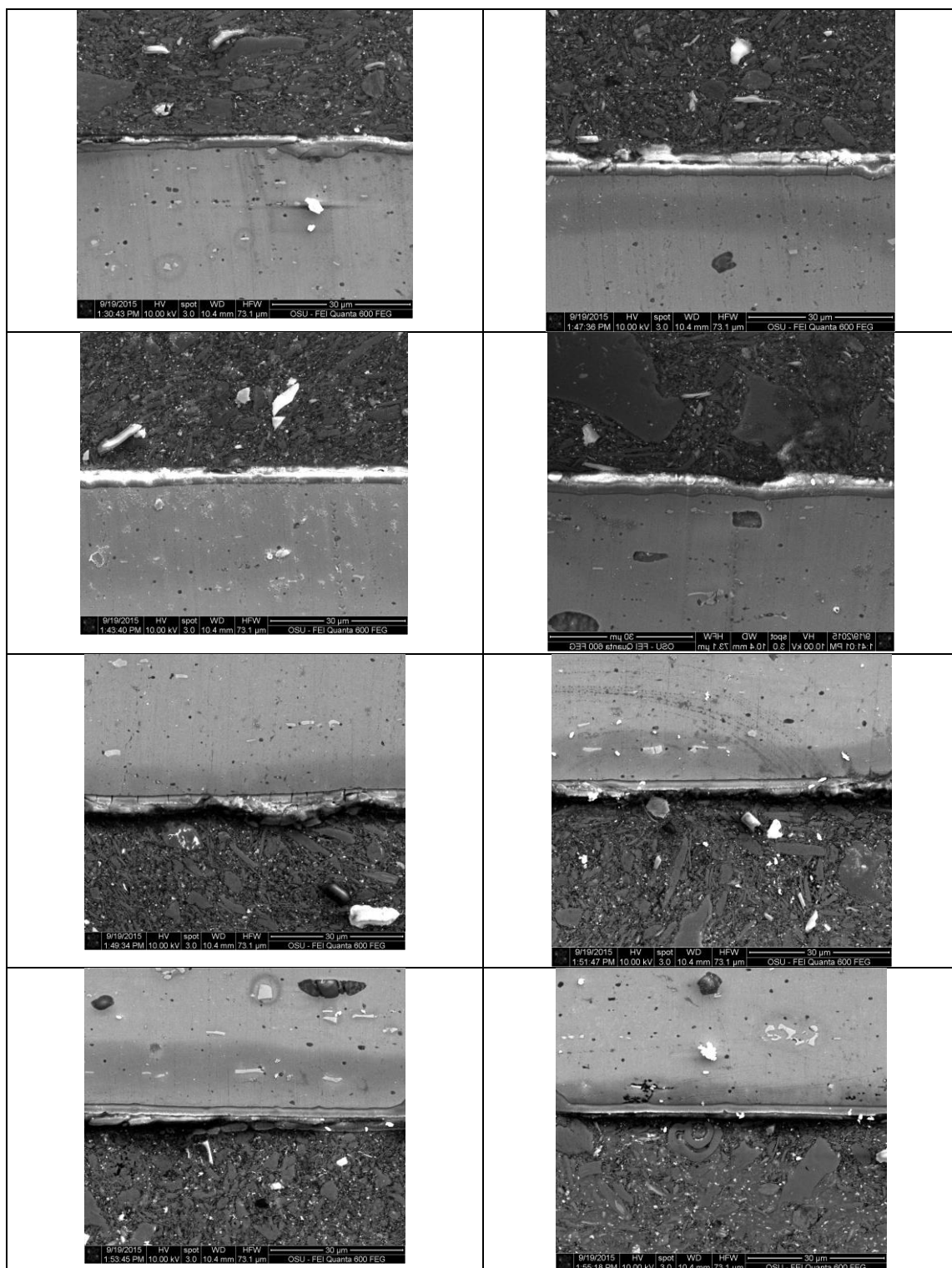
Figure 9.1. Cross-section images of original pre-filmed sample
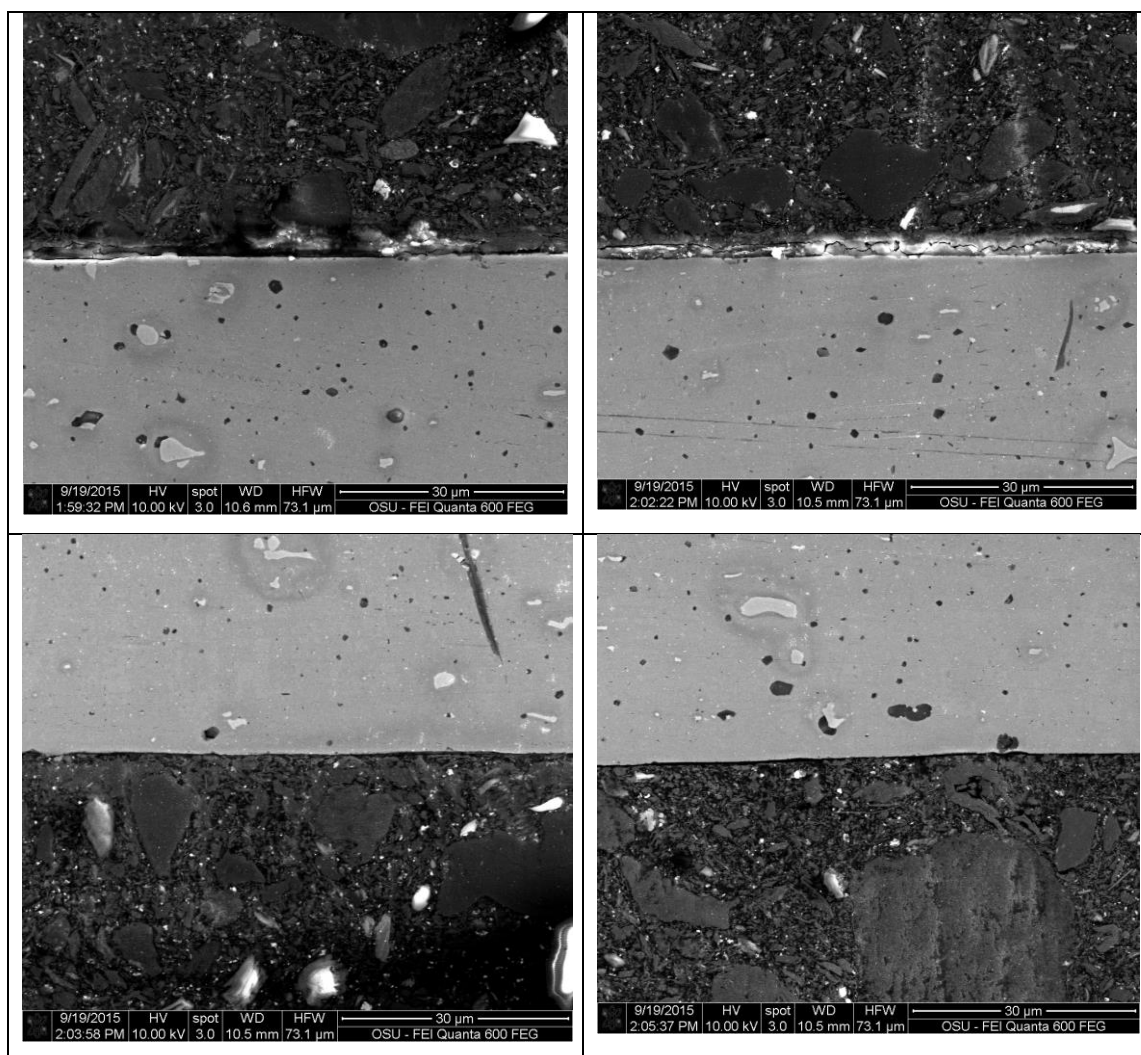
Figure 9.2. Cross-section of original non-pre-filmed sample
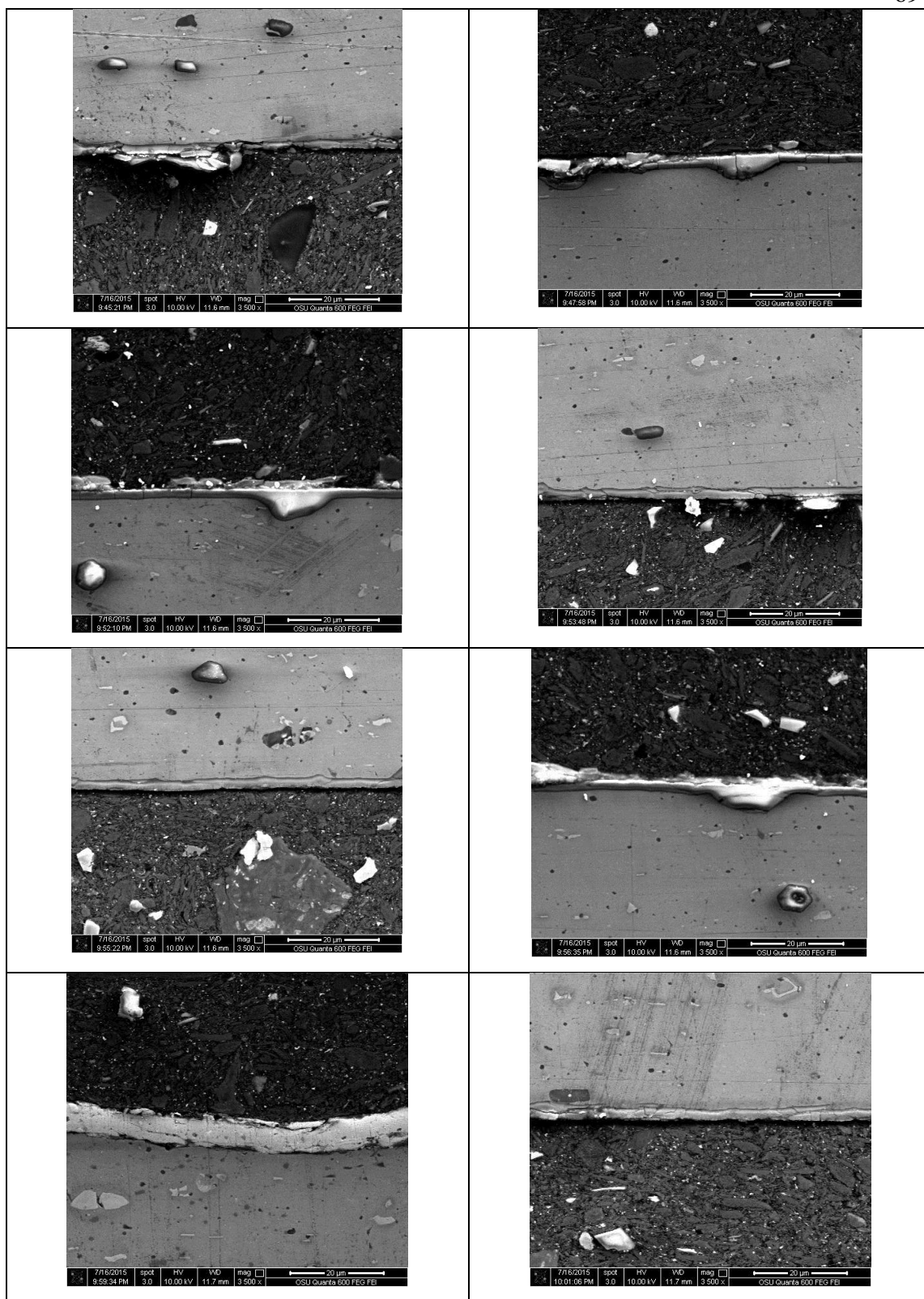
Figure 9.3. Cross-section of pre-filmed sample from first month
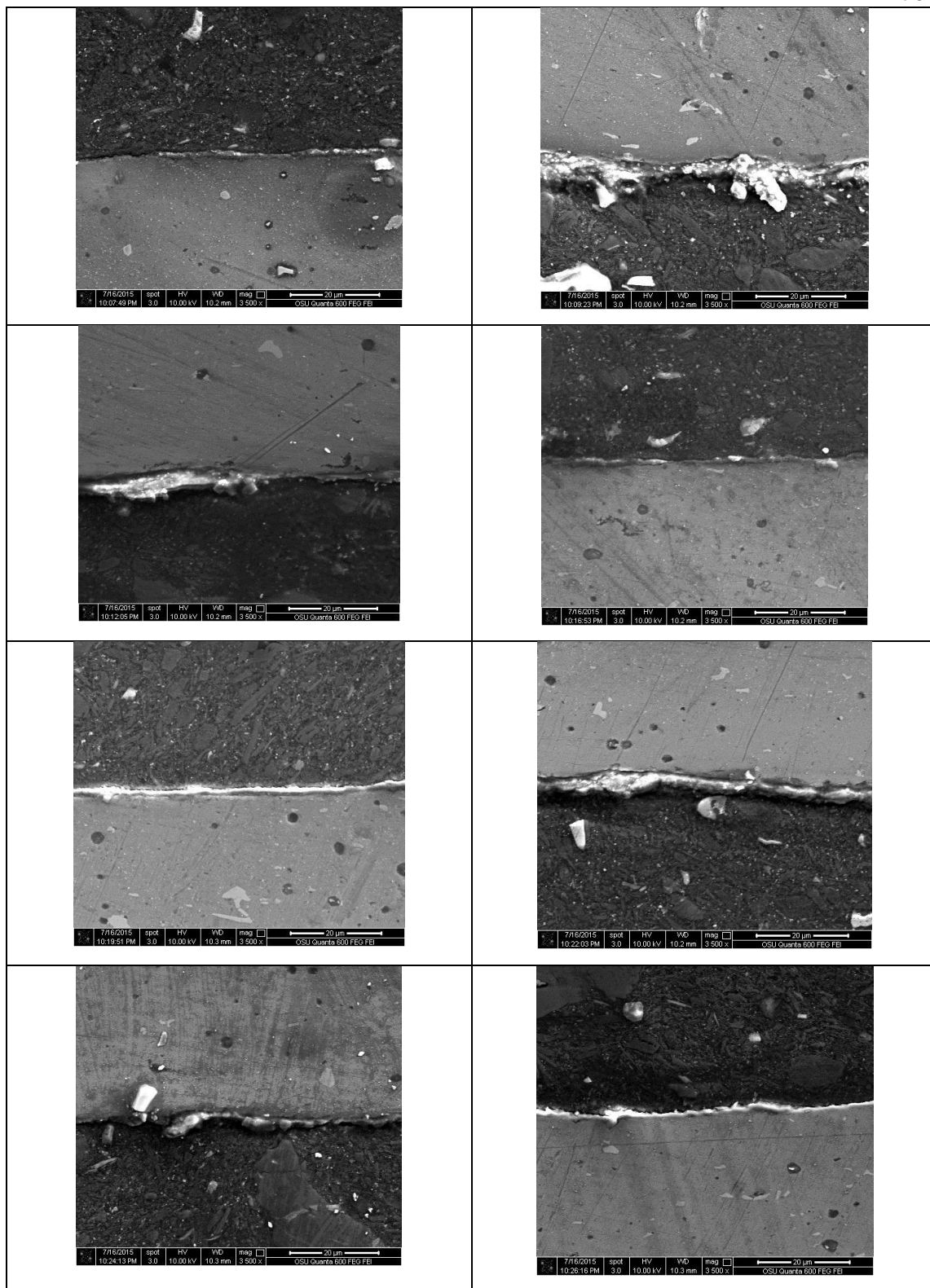
Figure 9.4. Cross-section of non-pre-filmed sample from first month
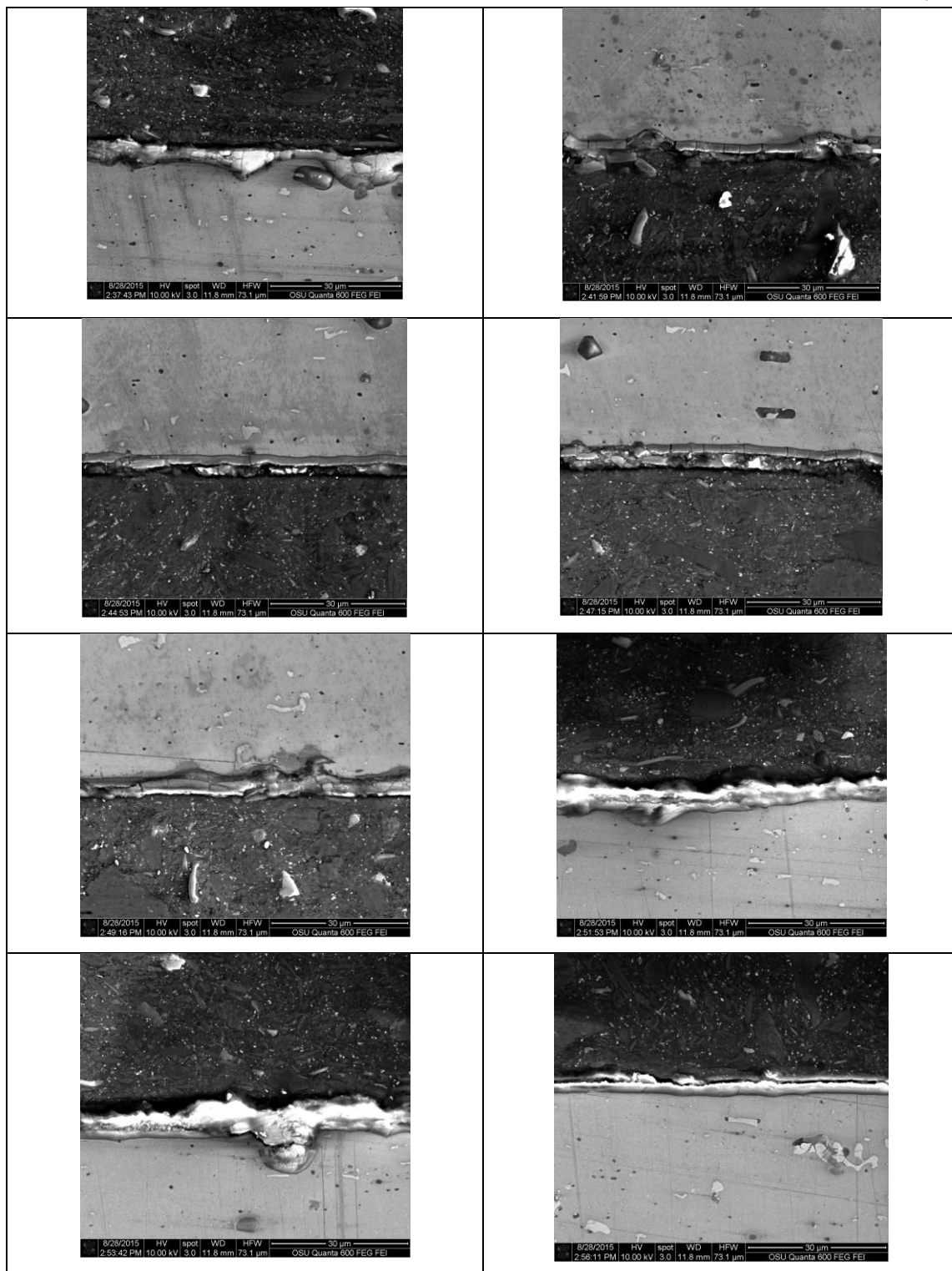
Figure 9.5. Cross-section of pre-filmed sample from second month
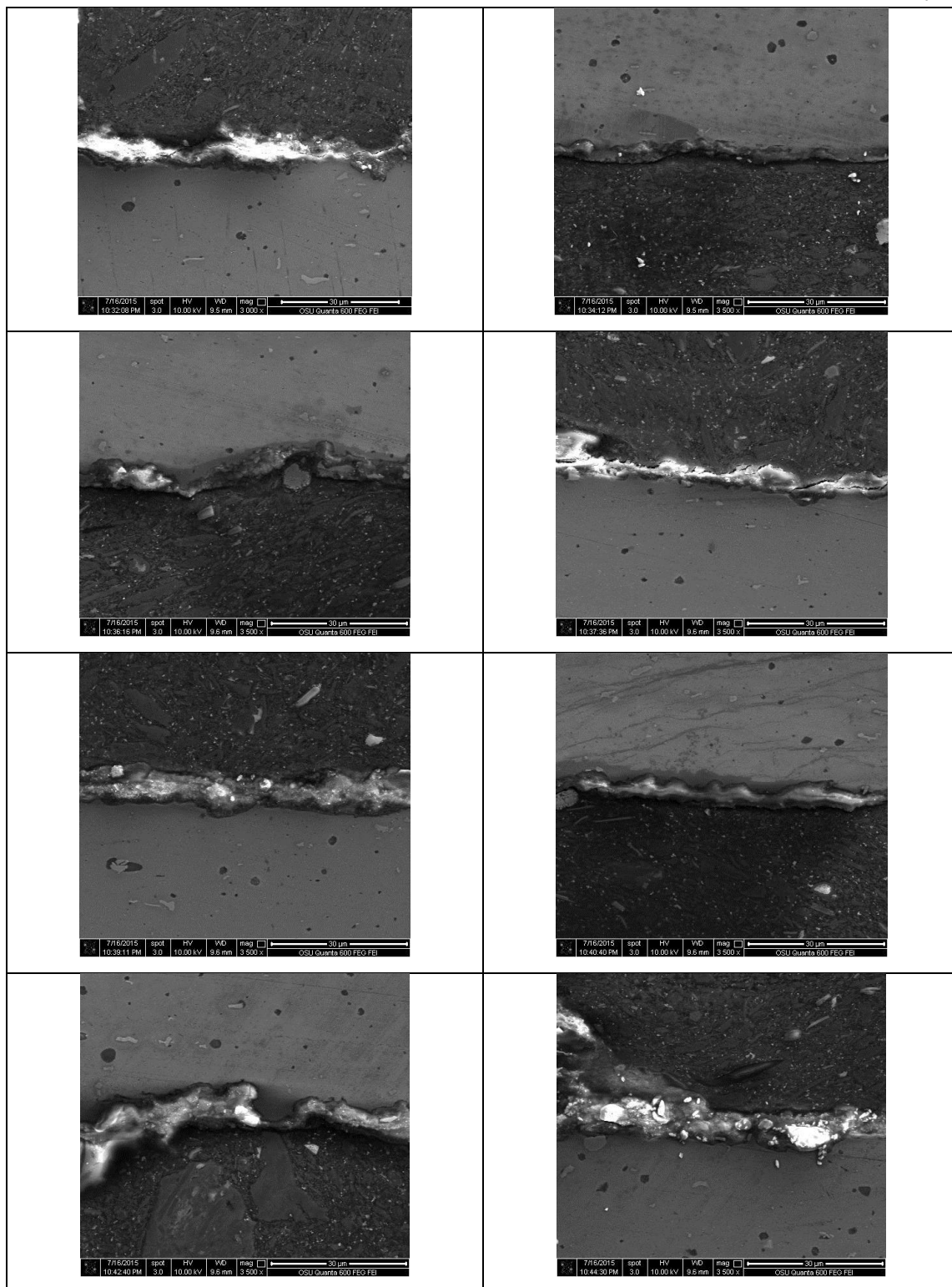
Figure 9.6. Cross-section of non-pre-filmed sample from second month
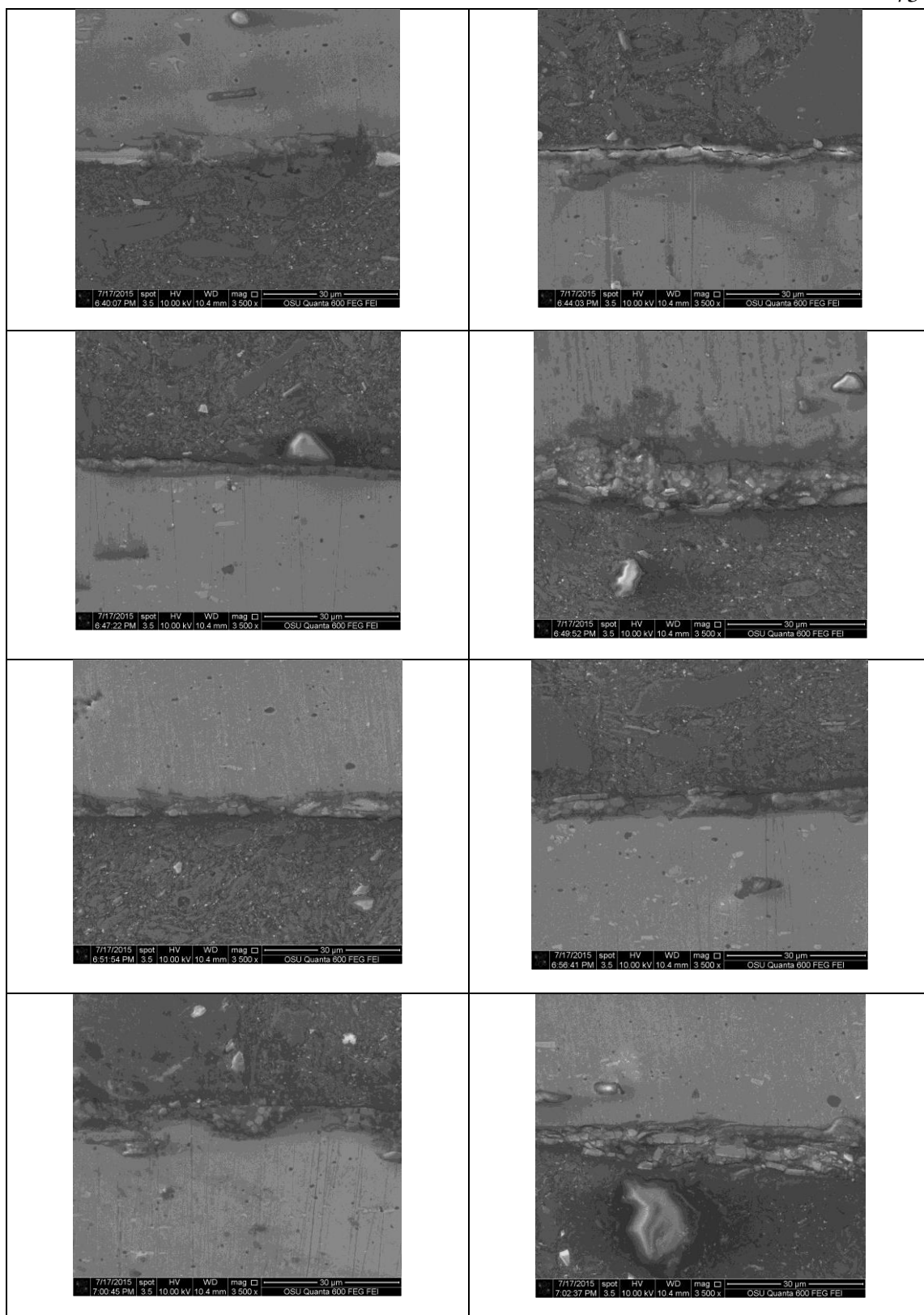
Figure 9.7. Cross-section of pre-filmed sample from third month
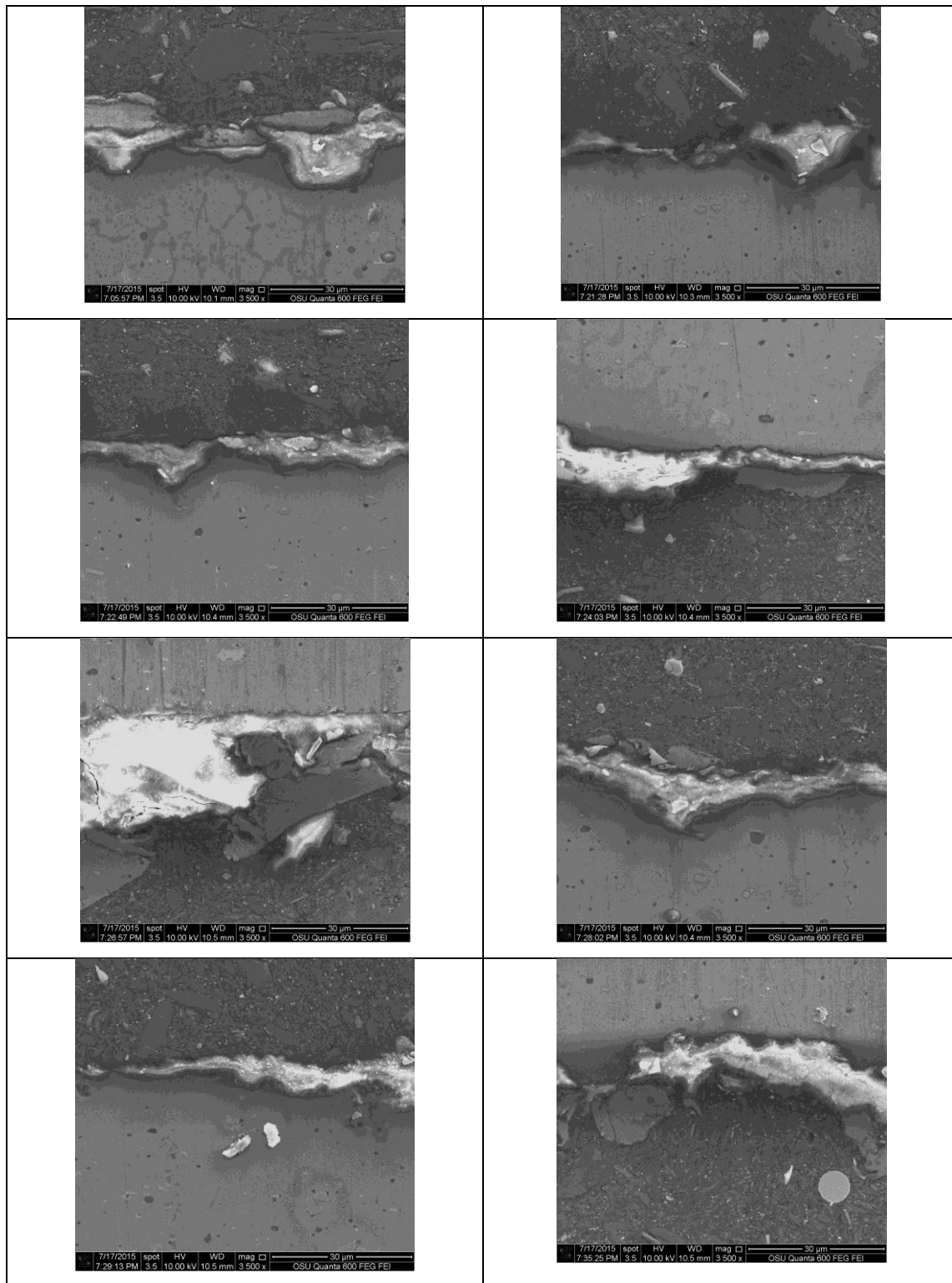
Figure 9.8. Cross-section of non-pre-filmed sample from third month
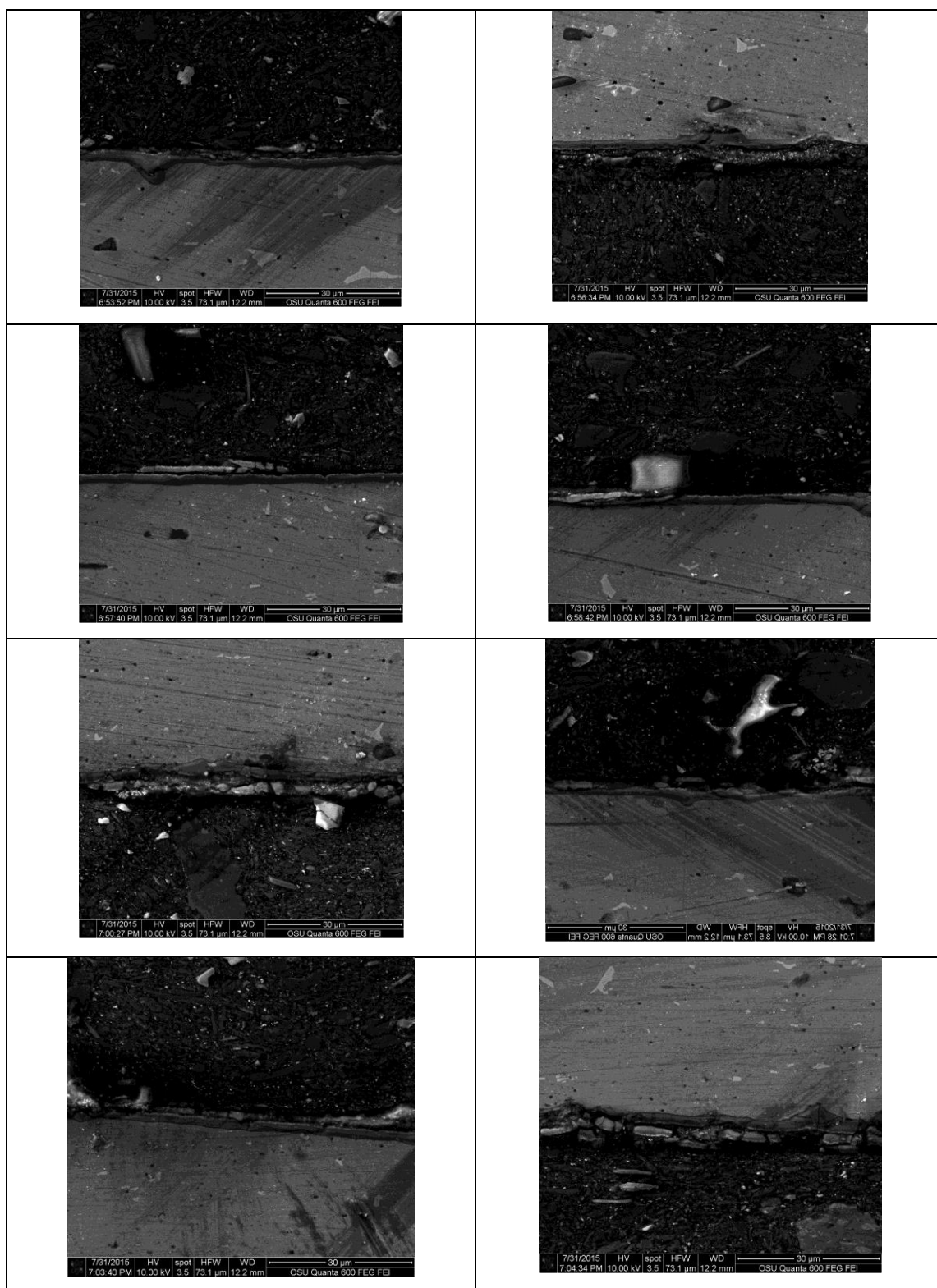
Figure 9.9. Cross-section of pre-filmed sample from fourth month
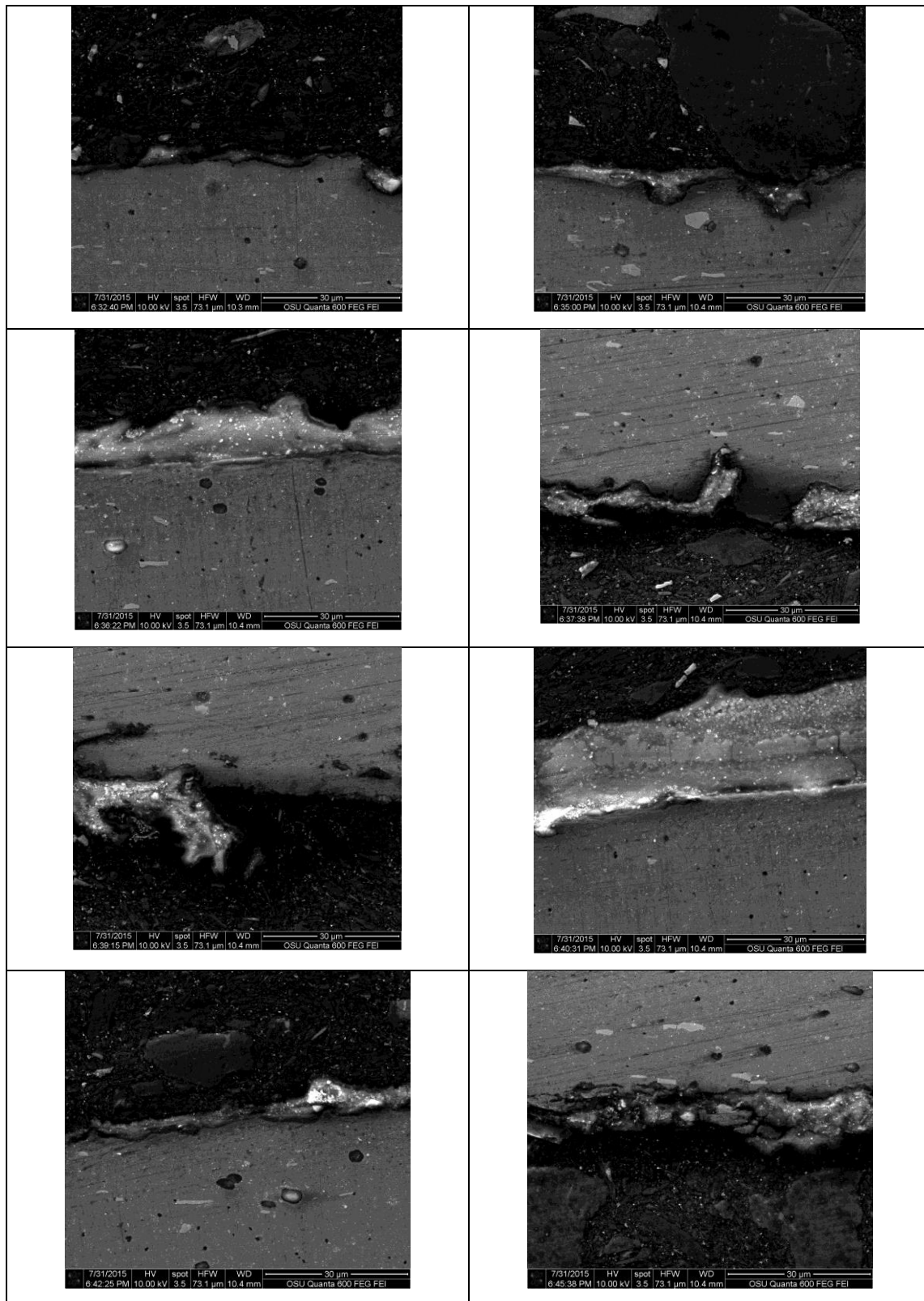
Figure 9.10. Cross-section of non-pre-filmed sample from fourth month
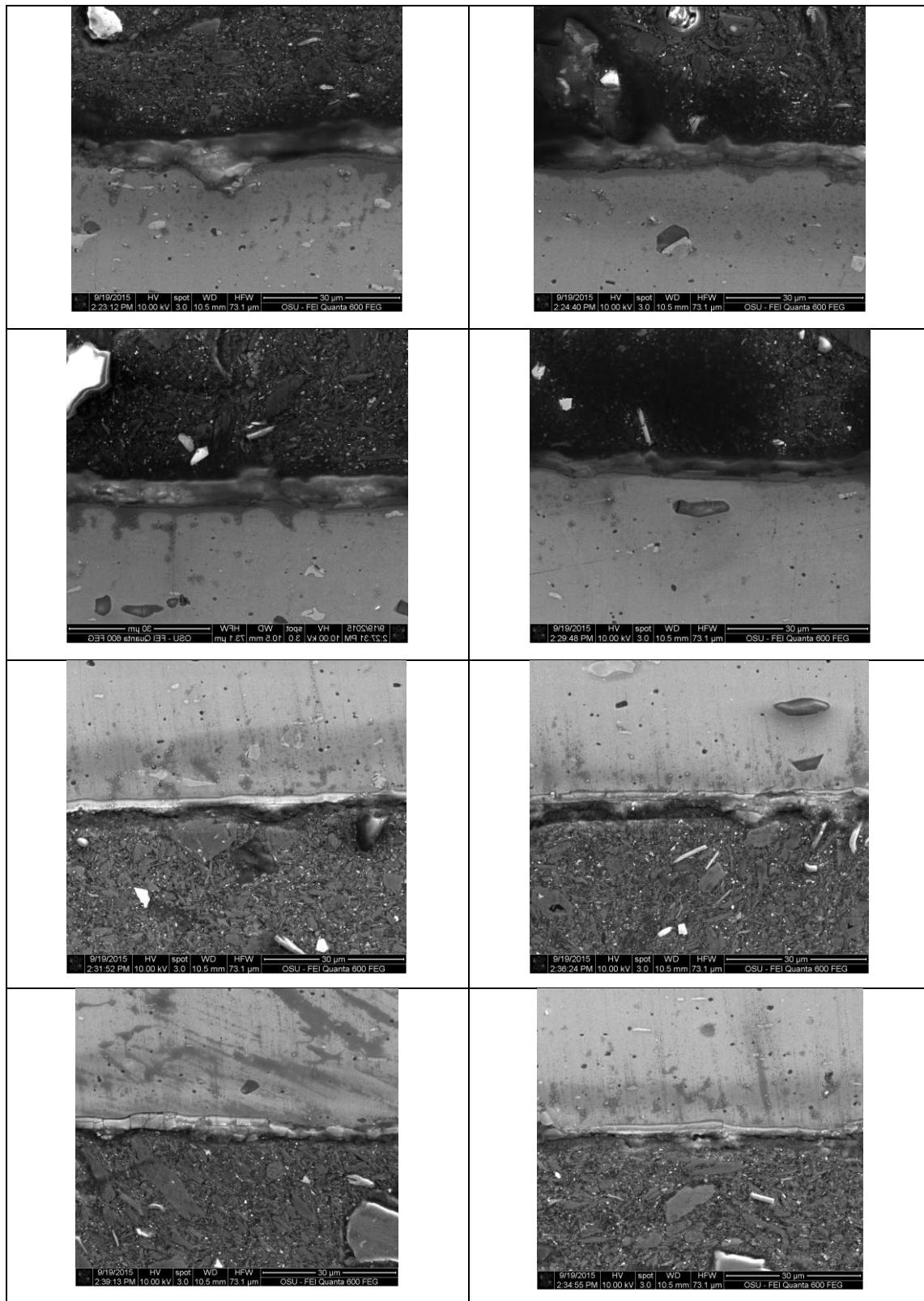
Figure 9.11. Cross-section of pre-filmed sample from fifth month
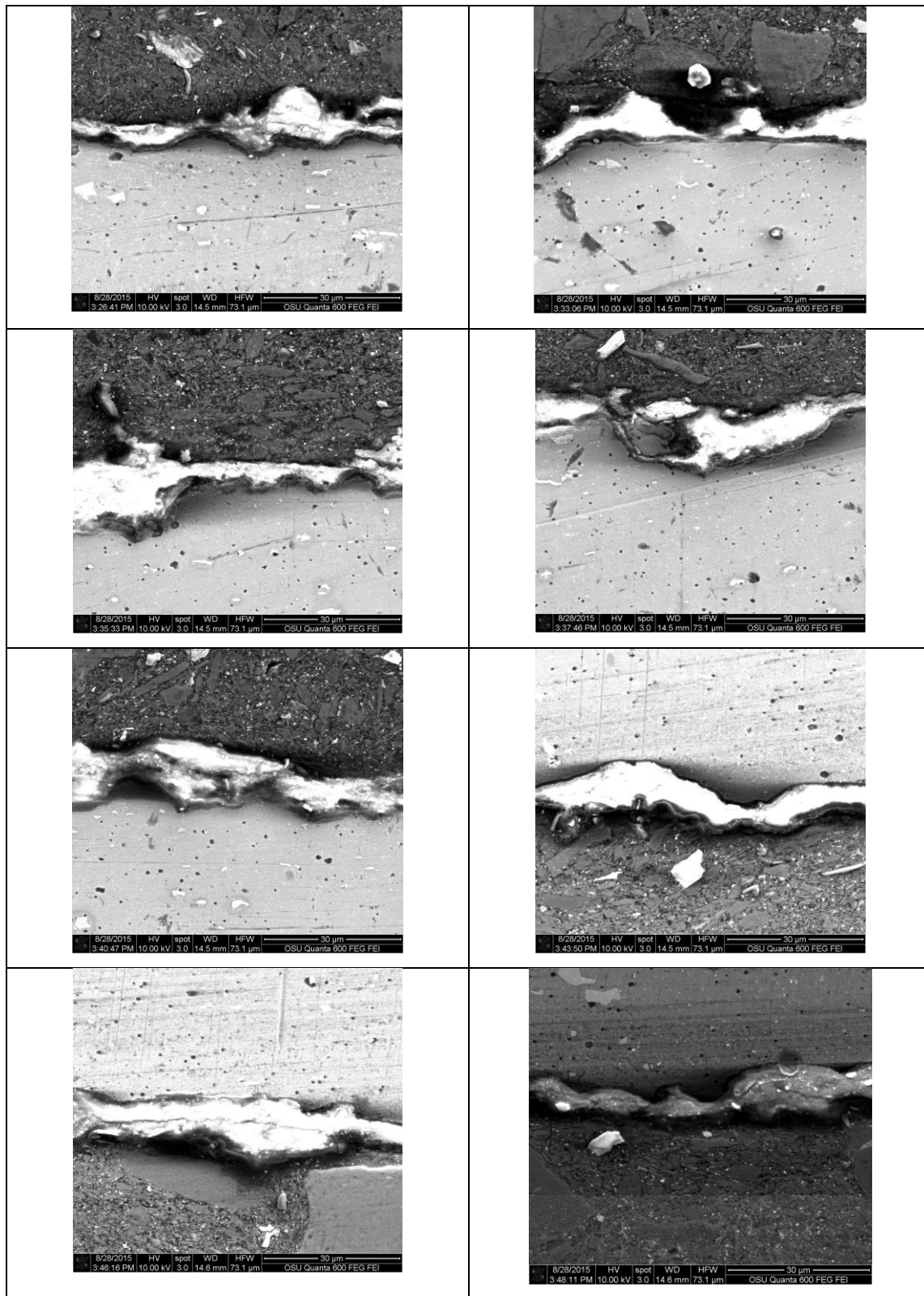
Figure 9.12. Cross-section of non-pre-filmed sample from fifth month
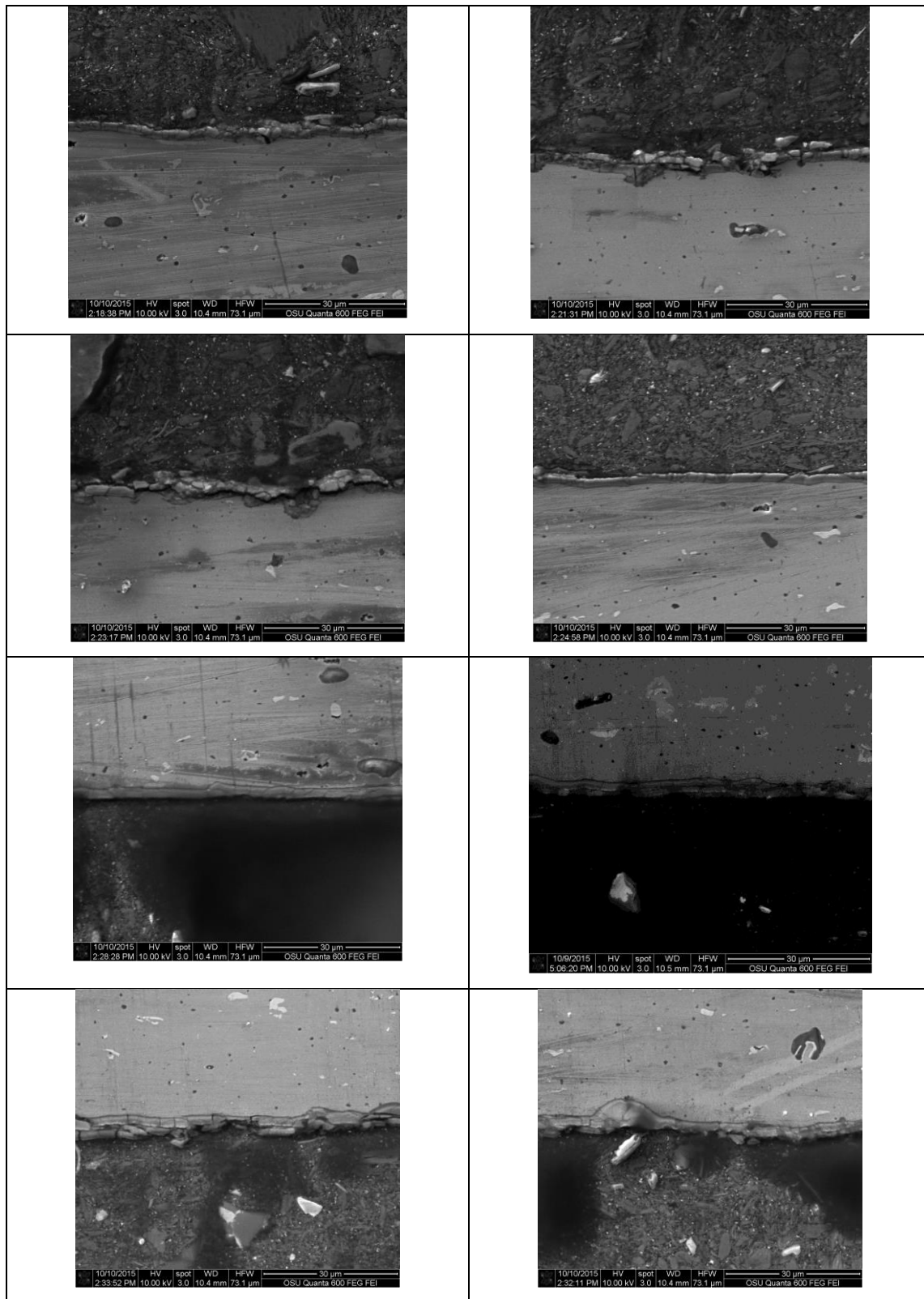
Figure 9.13. Cross-section of pre-filmed sample from sixth month
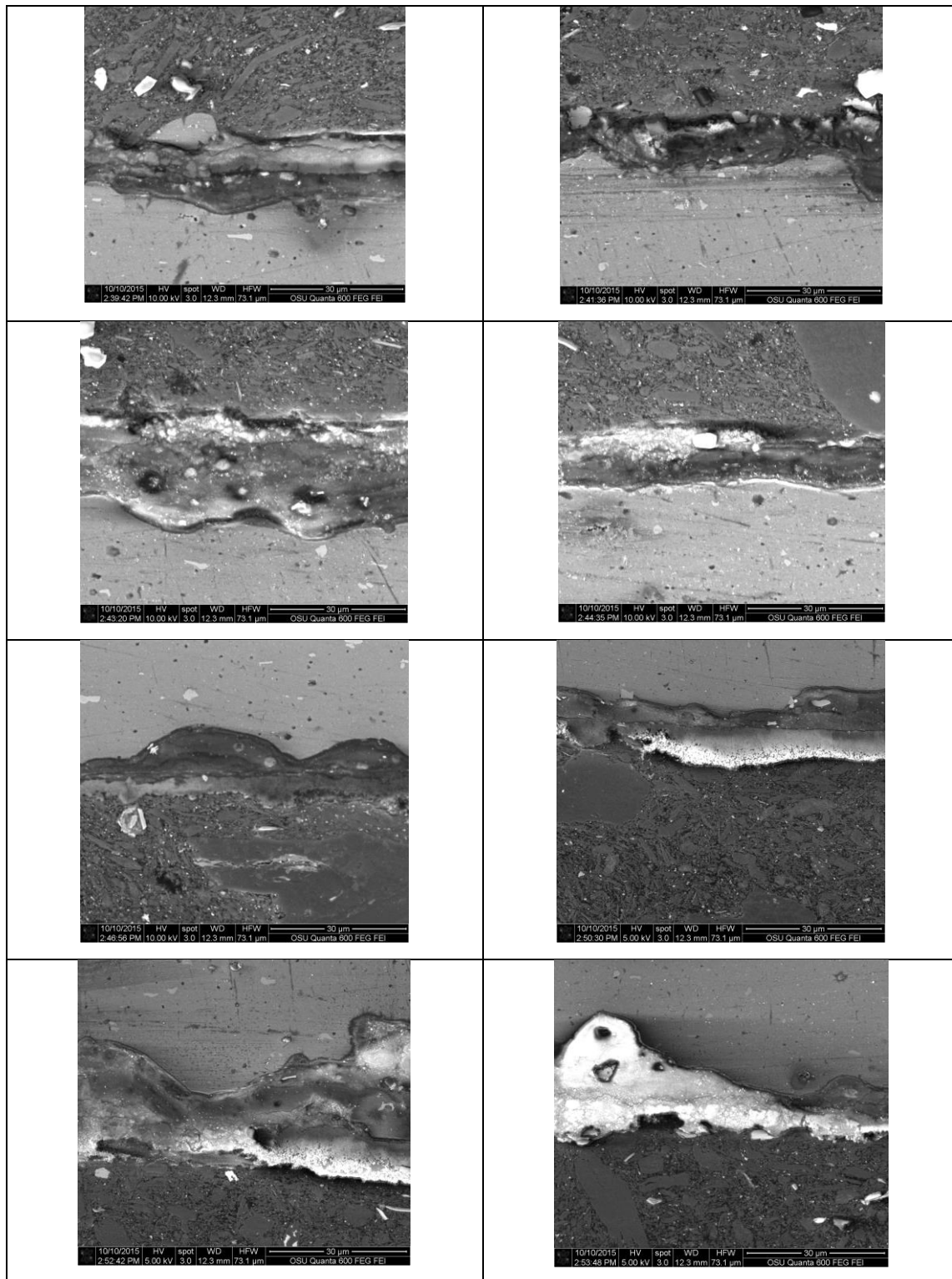
Figure 9.14. Cross-section of non-pre-filmed sample from sixth month

Pre-filmed samples' surfaces	Non-pre-filmed samples' surfaces
500X Original sample	500X Original sample
500X first month sample	500X first month sample
Second month	Second month
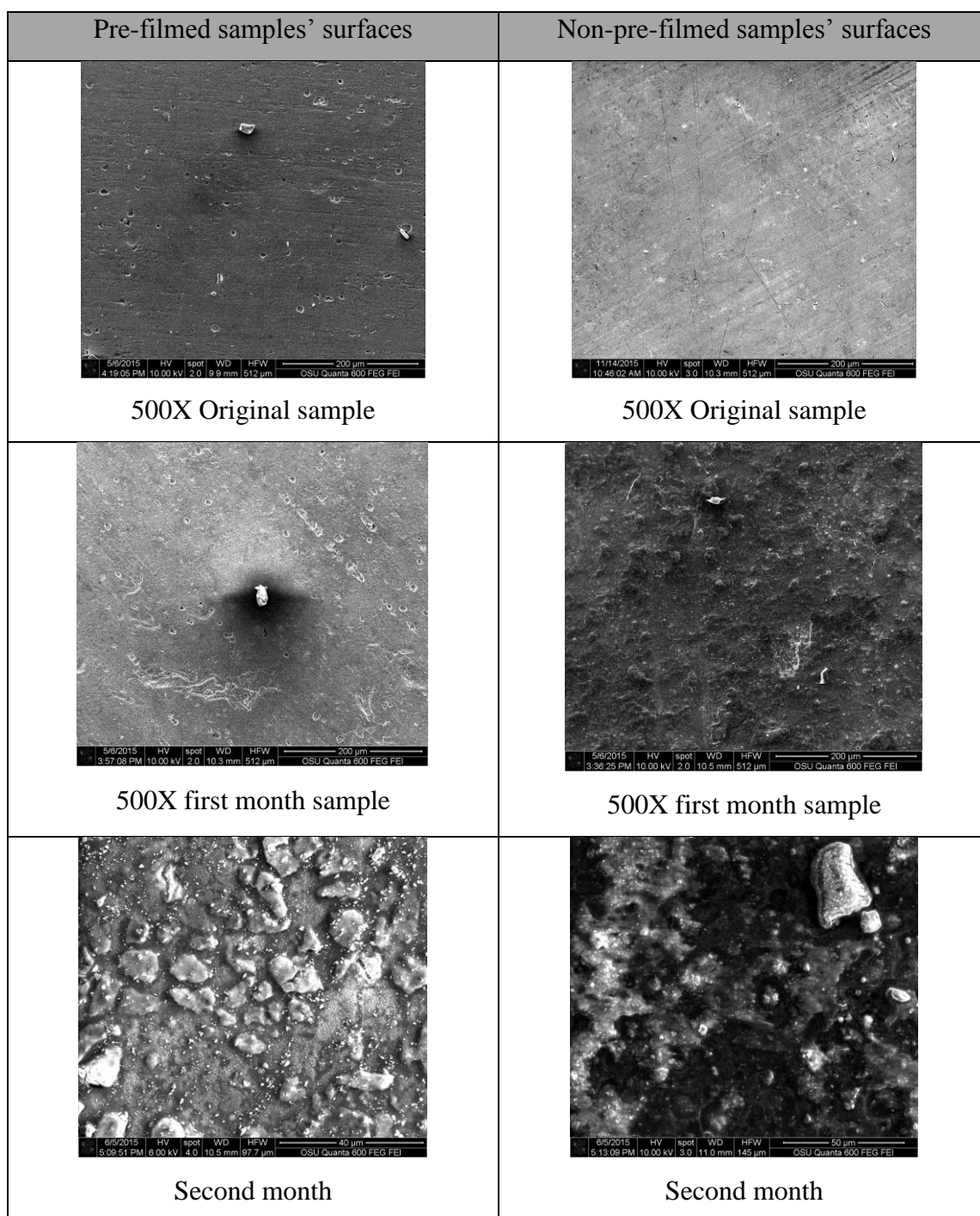
Figure 9.15. Surface SEM images from month one through three
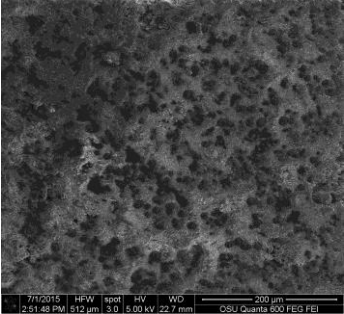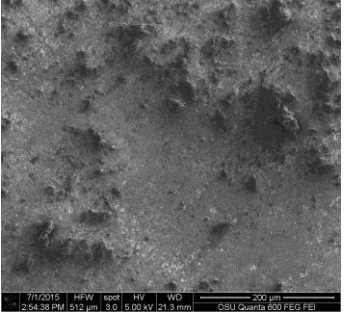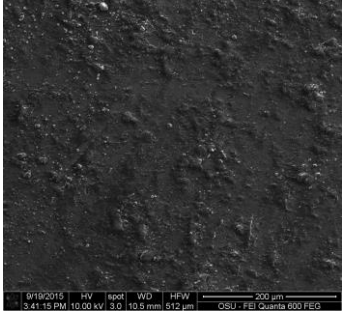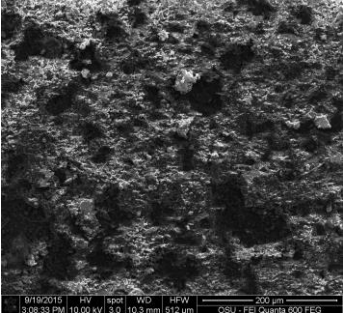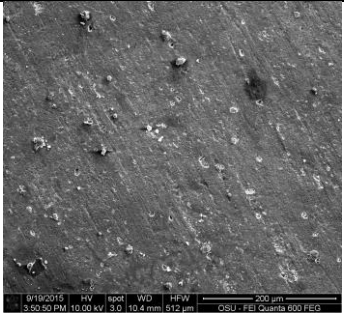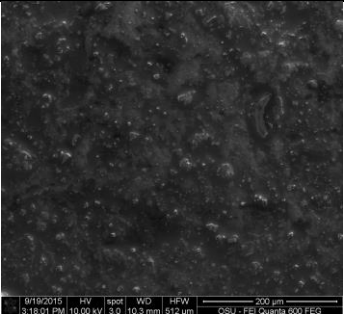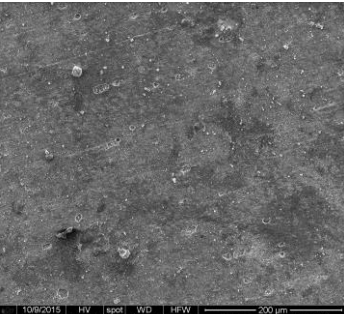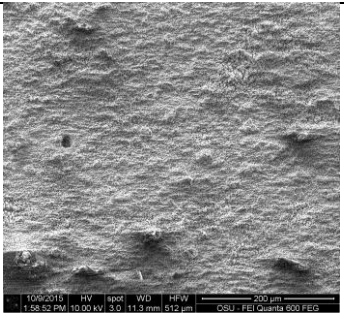
Pre-filmed samples' surfaces	Non-pre-filmed samples' surfaces
500X Deposit locaton from third month	500X from third month
500X from fourth month	550X from fourth month
500X from fifth month	500X from fifth month
500X from sixth month	500X from sixth month

Figure 9.16. Surface SEM images from month four through six

10 APPENDIX C –WATER CHEMICAL ANALYSIS.

Figure 10.1. Water chemical report

EDGE ANALYTICAL

Burlington, WA	Corporate Laboratory (a)	1620 S Walnut St	Burlington, WA 98233	800.735.9295 · 360.757.1400
Bellingham, WA	Microbiology (b)	805 Orchard Dr Ste 4	Bellingham, WA 98225	360.715.1212
Portland, OR	Microbiology/Chemistry (c)	9150 SW Pioneer Ct Ste W	Wilsonville, OR 97070	503.682.7802
Corvallis, OR	Microbiology (d)	540 SW Third Street	Corvallis, OR 97333	541.753.4946

Data Report

Client Name: Youran Wei
3235 NW Orchard Ave
Corvallis, OR 97330

Reference Number: **15-16632**
Project: Aluminum Alloy Corrosion

Report Date: 8/17/15

Date Received: 8/11/15
Approved by: mvp
Authorized by:

Sarah P Miller
Lab Manager, Corvallis

| Sample Description: EFL Test Loop - Radiation Center | | | | | | | | Sample Date: 8/11/15 10:45 am | |
| Lab Number: 36923 | Sample Comment: | | | | | | | Collected By: Youran Wei | |

CAS ID#	Parameter	Result	PQL	MDL	Units	DF	Method	Lab	Analyzed	Analyst	Batch	Comment
7631-86-9	SILICA	9.58	0.05	0.003	mg/L	1.0	200.7	a	8/14/15	BJ	200.7_150814A	

Notes:

ND = Not detected above the listed practical quantitation limit (PQL) or not above the Method Detection Limit (MDL), if requested.
PQL = Practical Quantitation Limit is the lowest level that can be achieved within specified limits of precision and accuracy during routine laboratory operating conditions.
D.F. - Dilution Factor

If you have any questions concerning this report contact us at the above phone number.
Form: cRpt_2.rpt

Figure 10.2. Silica test